AD-762 210

COMPARISON OF ANALYTICALLY AND EXPERIMENTALLY DETERMINED DYNAMIC BEHAVIOR OF TETHERED BALLOONS

Jerome J. Vorachek, et al

Goodyear Aerospace Corporation

Prepared for:

Air Force Cambridge Research Laboratories

30 March 1973

AFCRL-TR-73-0284

COMPARISON OF ANALYTICALLY AND EXPERIMENTALLY DETERMINED DYNAMIC BEHAVIOR OF TETHERED BALLOONS

by

Jerome J. Vorachek
George R. Doyle, Jr.

Goodyear Aerospace Corporation
Akron, Ohio 44315

Contract No. F19628-72-C-0219
Project No. 6665
Task No. 666509
Work Unit No. 66650901

Scientific Report No. 1
30 March 1973

Contract Monitor: Don E. Jackson, Capt. USAF
Aerospace Instrumentation Laboratory

Prepared for

AIR FORCE CAMBRIDGE RESEARCH LABORATORIES
AIR FORCE SYSTEMS COMMAND
UNITED STATES AIR FORCE
BEDFORD, MASSACHUSETTS 01730

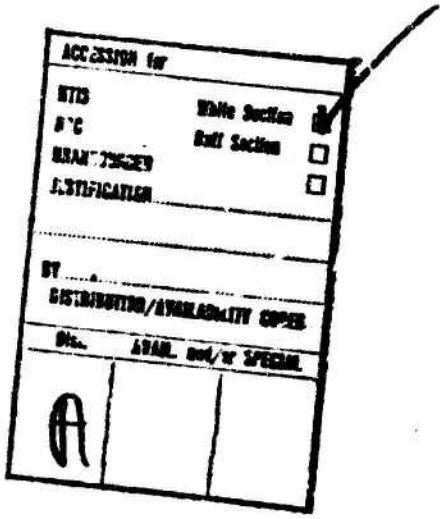

Qualified requestors may obtain additional copies from the Defense Documentation Center. All others should apply to the National Technical Information Service.

UNCLASSIFIED
Security Classification

DOCUMENT CONTROL DATA - R & D

(Security classification of title, body of abstract and indexing annotation must be entered when the overall report is classified)

1. ORIGINATING ACTIVITY (Corporate author)	2a. REPORT SECURITY CLASSIFICATION
Goodyear Aerospace Corporation 1210 Massillon Road Akron, Ohio 44315	Unclassified
	2b. GROUP

3. REPORT TITLE

COMPARISON OF ANALYTICALLY AND EXPERIMENTALLY DETERMINED DYNAMIC BEHAVIOR OF TETHERED BALLOONS

4. DESCRIPTIVE NOTES (Type of report and inclusive dates)

Scientific. Interim.

5. AUTHOR(S) (First name, middle initial, last name)

Jerome J. Vorachek
George R. Doyle, Jr.

6. REPORT DATE	7a. TOTAL NO. OF PAGES	7b. NO. OF REFS
30 March 1973	269	11

8a. CONTRACT OR GRANT NO	9a. ORIGINATOR'S REPORT NUMBER(S)
F19628-72-C-0219	GER 15932 Scientific Report No. 1
b. PROJECT NO. 6665-09-01	
c. DoD Element 62101F	9b. OTHER REPORT NO(S) (Any other numbers that may be assigned this report)
d. DoD Subelement 686665	AFCRL-TR-73-0284

10. DISTRIBUTION STATEMENT

A - Approved for public release; distribution unlimited.

11. SUPPLEMENTARY NOTES	12. SPONSORING MILITARY ACTIVITY
TECH, OTHER	Air Force Cambridge Research Laboratories (LC) L. G. Hanscom Field Bedford, Massachusetts 01730

13. ABSTRACT

Mathematical tools were developed previously to analyze the dynamic behavior of tethered balloon systems. The model for the tethered balloon system consists of the streamlined balloon and a tether made up of three discrete links. The tools consist of the linearized characteristic equations which incorporate the physical, aerodynamic and mass characteristics of the system and the dynamic simulation computer program which determines the response of the tethered balloon system to wind disturbances. A tethered balloon system consisting of a 70,000 cubic foot aerodynamically shaped balloon and a 0.52 inch diameter Nolaro tether was flown at Fair Site on White Sands Missile Range to obtain experimental motion data. Experimental test conditions and test tethered balloon system characteristics were input in the computer programs and balloon dynamic behavior was predicted. A comparison of experimental and predicted dynamic characteristics of the tethered balloon showed a reasonable match although some discrepancies existed. In spite of these, it is concluded that the stability and dynamic simulation computer programs are a powerful tool for design and analysis of tethered balloon systems.

DD FORM 1 NOV 65 1473

UNCLASSIFIED
Security Classification

14 KEY WORDS	LINK A		LINK B		LINK C	
	ROLE	WT	ROLE	WT	ROLE	WT
Aerostats						
Balloons						
Balloon Aerodynamics						
Balloon Dynamics						
Balloon Behavior						
Balloon Flying Qualities						
Balloon Mass Characteristics						
Balloon Stability						
Balloon Systems						
Cables						
Cable Dynamics						
Captive Balloons						
Dynamic Simulation Analysis						
Kite Balloons						
Stability Analysis						
Tethered Balloons						
Tethered LTA Vehicles						
Tethers						

AFCRL-TR-73-0284

COMPARISON OF ANALYTICALLY AND EXPERIMENTALLY DETERMINED DYNAMIC BEHAVIOR OF TETHERED BALLOONS

by

Jerome J. Vorachek
George R. Doyle, Jr.

Goodyear Aerospace Corporation
Akron, Ohio 44315

Contract No. F19628-72-C-0219
Project No. 6665
Task No. 666509
Work Unit No. 66650901

Scientific Report No. 1
30 March 1973

Contract Monitor: Don E. Jackson, Capt. USAF
Aerospace Instrumentation Laboratory

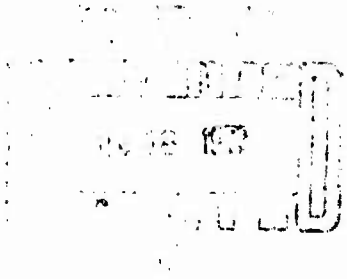

Approved for public release; distribution unlimited

Prepared for

AIR FORCE CAMBRIDGE RESEARCH LABORATORIES
AIR FORCE SYSTEMS COMMAND
UNITED STATES AIR FORCE
BEDFORD, MASSACHUSETTS 01730

ABSTRACT

Mathematical tools were developed previously to analyze the dynamic behavior of tethered balloon systems. The model for the tethered balloon system consists of the streamlined balloon and a tether made up of three discrete links. The tools consist of the linearized characteristic equations which incorporate the physical, aerodynamic and mass characteristics of the system and the dynamic simulation computer program which determines the response of the tethered balloon system to wind disturbances. A tethered balloon system consisting of a 70,000 cubic foot aerodynamically shaped balloon and a 0.52 inch diameter Nolaro tether was flown at Fair Site on White Sands Missile Range to obtain experimental motion data. Experimental test conditions and test tethered balloon system characteristics were input in the computer programs and balloon dynamic behavior was predicted. A comparison of experimental and predicted dynamic characteristics of the tethered balloon showed a reasonable match although some discrepancies existed. In spite of these, it is concluded that the stability and dynamic simulation computer programs are a powerful tool for design and analysis of tethered balloon systems.

TABLE OF CONTENTS

LIST OF ILLUSTRATIONS

LIST OF ILLUSTRATIONS (cont.)

LIST OF TABLES

SECTION I

INTRODUCTION

The objective of the present program is to compare actual flight data with analytically predicted data for a tethered balloon and to improve the mathematical model if required. A second objective is to study the dynamic behavior of two tethered balloon types

Mathematical tools have been developed on a previous program to analyze the dynamic behavior of tethered balloon systems. The techniques used are determination of the roots of the linearized characteristics equations which incorporate the physical, aerodynamic, and mass characteristics of the system, and dynamic simulation of the tethered balloon systems to determine response of the systems to wind disturbances. The techniques are complementary and each helps to obtain insight into the behavior of tethered balloon systems.

The model for the tethered balloon system consists of the streamlined balloon and a tether made up of three discrete links. The derivation of non-linear equations of motion for this system were devised in three dimensions. The equations are linearized for stability analysis and treated as uncoupled in the longitudinal and lateral degrees of freedom. Characteristic equations of the system are developed and solved for the roots which represent the frequency and damping qualities. References 1, 2, and 3 document the results of this program.

A tethered balloon system consisting of a 70,000 cubic foot aerodynamically shaped balloon and a .52 inch diameter Nolaro tether was flown by AFCRL at White Sands Missile Range to obtain experimental balloon motion data. These experimental data have been compared with those predicted by the mathematical model. The efforts to establish the validity of the analytical techniques are reported herein.

SECTION II

TECHNIQUES FOR STUDY OF DYNAMIC BEHAVIOR OF TETHERED BALLOONS

A. MATHEMATICAL MODELS

A system of differential equations was developed (see References 2 and 3) that describes the motion of the tethered balloon in three dimensions. The degrees of freedom associated with the motion are yaw, pitch and roll of the balloon about its dynamic mass center, and pitch and yaw (lateral rotation) of the tether. There are a total of 3 + 2N degrees of freedom where N is the number of links used to simulate the tether.

First consider the longitudinal degrees of freedom. The dependent variables shown in Figure 1 are θ (pitch of the balloon) and ζ_r (pitch of the "r"th link), where r is a particular link. All angles are shown positive.

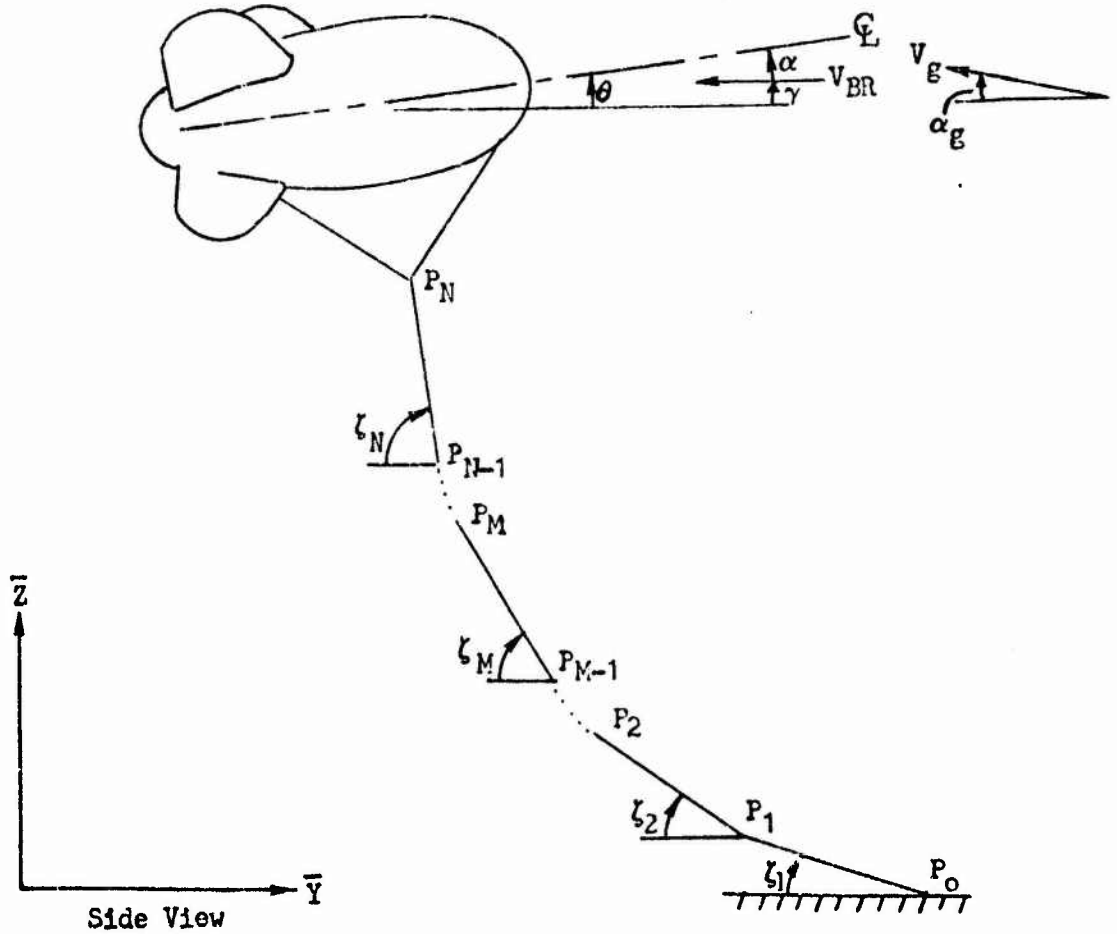

Figure 1. Balloon Tether Model in Longitudinal Plane

In Figure 1 V_{BR} is the relative velocity of the balloon's center of gravity with respect to the air and is the resultant of the steady wind, the wind gust, the balloon translational motion and the velocity due to rotation of the balloon about its center of mass. The angle of attack (α) is the angle that the relative wind forms with the longitudinal axis of the balloon.

The lateral degrees of freedom are displayed in Figure 2 which gives the front and top view of the tethered balloon. The lateral degrees of freedom are: ψ(yaw of balloon), ϕ (roll of balloon), and σ_r (yaw of "r"th link). All angles are shown positive).

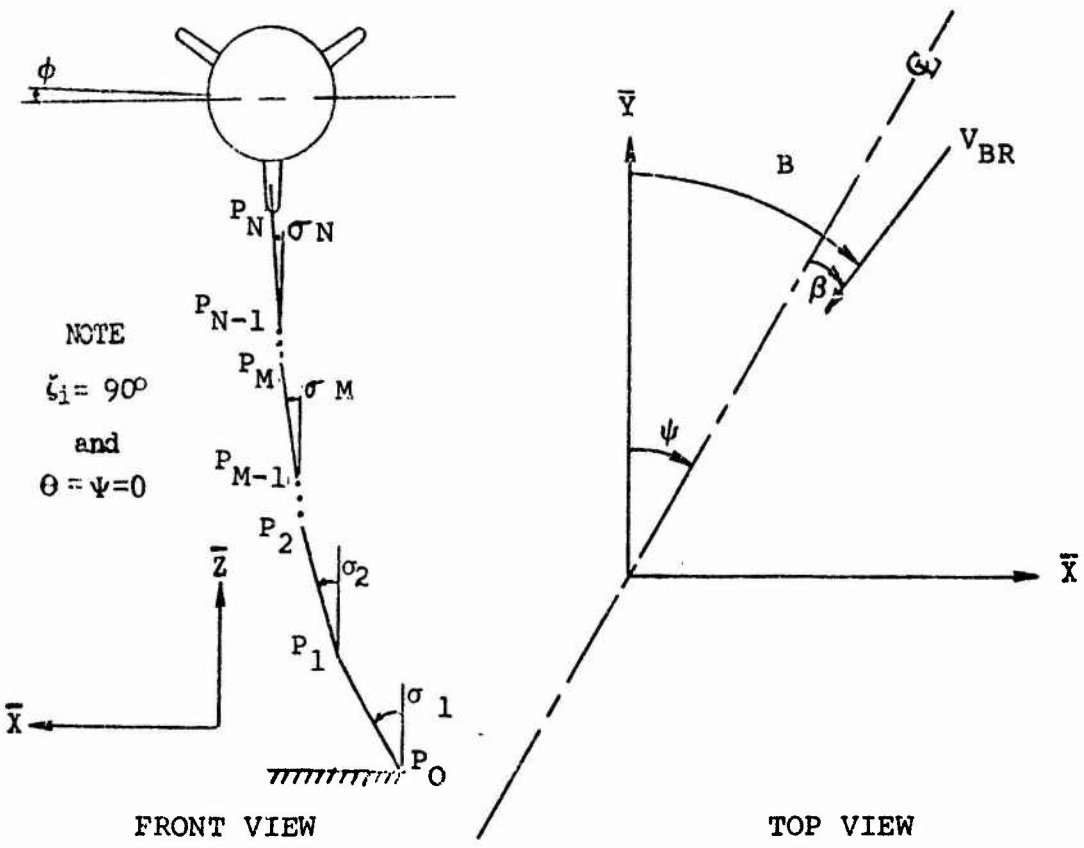

Figure 2. Balloon Tether Model in Lateral Plane

Pertinent geometry of the tethered balloon and applied forces are identified in Figure 3.

In order to separate the equations of motion into a longitudinal response and a lateral response, it was further assumed that the system was near equilibrium. This resulted in a set of equations describing the longitudinal motion which is coupled only in the pitching variables of the balloon and the pitching variables of the tether. However, the second set of equations for the lateral motion does not completely uncouple from the longitudinal degrees of freedom because the

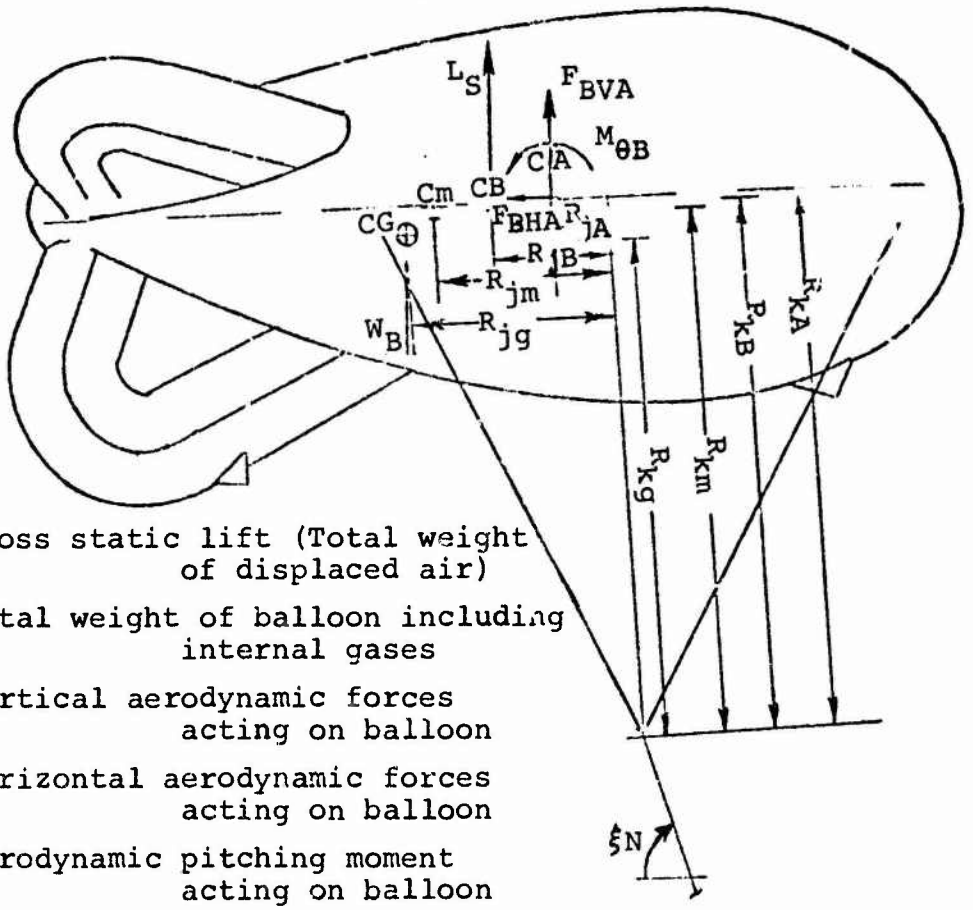

L_S - Gross static lift (Total weight of displaced air)

W_B - Total weight of balloon including internal gases

F_{BVA} - Vertical aerodynamic forces acting on balloon

F_{BHA} - Horizontal aerodynamic forces acting on balloon

$M_{\theta B}$ - Aerodynamic pitching moment acting on balloon

CA - Aerodynamic reference center

CB - Center of buoyancy of total displaced volume

Cm - Apparent mass center and dynamic center in pitch (and yaw)

CG - Center of gravity of total weight of balloon

Figure 3. Balloon Geometry and Applied Forces

equilibrium angles in the longitudinal plane are not zero. Therefore, when solving the lateral degrees of freedom, it must be assumed that the longitudinal variables remain constant and equal to their equilibrium values. In both the longitudinal and lateral cases, the tether is simulated by three rigid links. The number of uncoupled dynamic equations is four for the longitudinal response and five for the lateral response.

B. GENERAL STABILITY THEORY

The equilibrium configuration of a tethered balloon can be defined as that position which demands that the summation of all applied moments equals zero. The equilibrium is said to be stable if, for any small disturbance, the system ultimately returns to its equilibrium conditions. Two types of stability are of interest. In the first (statically stable), a small displacement of the system will create forces which tend to return the system to its equilibrium position. The second (dynamically stable) produces a motion which eventually restores equilibrium. If the motion is periodic, it is characterized by a damped frequency and a damping ratio. Similar definitions apply for statically and dynamically unstable motions. A third possibility is for the system to be neutrally stable during which the motion neither diverges nor converges.

Characteristic equations were derived for study of the stability of this system. The general approach was as follows:

(1) Derive the nonlinear equations of motion in three dimensions for each degree-of-freedom

(2) Assume the motion is near equilibrium so that the equations can be linearized and separated into a longitudinal motion and a lateral motion

(3) Laplace transform the linear equations from the time domain to the "S" domain assuming that the initial conditions are zero. This establishes a matrix equation of the following form:

$$[A] \{X(S)\} = \{0\} \qquad (1)$$

where $\{X(S)\}$ is the eigenvector and [A] is a square matrix whose elements are quadratics in S containing the physical properties of the system.

(4) Expand the determinant of [A] such that the characteristic polynominal is obtained.

Each root of the characteristic equation represents a term in the general solution of the form, $A_i e^{S_i t}$, where S_i is the "i"th root and A_i is an amplitude, dependent on the initial conditions of the system. Both real and complex roots may appear where the complex roots occur in conjugate pairs. In general for "n" degrees of freedom, the characteristic equation will yield "2n" roots. Each pair of complex conjugate roots represents one oscillatory motion, while each real root represents one aperiodic motion.

First consider an oscillatory system. This motion is characterized by two roots of the form $S_i = X \pm i\,Y$, where X and Y are real numbers and $i = \sqrt{-1}$. Several important quantities can be found from the root. The natural frequency associated with this motion is $\omega_n = \sqrt{X^2 + Y^2}$. The damping ratio is $\zeta = \frac{-X}{\omega_n}$. The damping frequency is $\omega_d = \omega_n\sqrt{1 - \zeta^2} = Y$. It is also of interest to know the time to half amplitude for a stable root or the time to double amplitude for an unstable root. This quantity can easily be found by considering one oscillatory motion. The general solution for free vibration is

$$Z = Ce^{-\zeta\,\omega_n t} \sin(\omega_d t + \phi) \qquad (2)$$

where ϕ is the phase angle dependent upon initial conditions

C is a constant dependent upon initial conditions

The half amplitude time is

$$t_2 - t_1 = \frac{0.693}{\zeta\omega_n} \qquad (3)$$

The second possibility is an aperiodic motion given by the expression

$$Z = Ce^{Xt} \qquad (4)$$

where X is the real part of one root and the imaginary part (Y) is zero

If X is negative, Z approaches zero as time increases indefinitely and the motion is said to be overdamped. Like the oscillatory motion, roots which give overdamped motions will also occur in pairs. However, unlike the complex conjugate roots which result in one oscillatory motion, each real root is a distinct motion. Therefore, it is possible for an "n" degree-of-freedom system to have "2n" distinct motions if the system is so heavily damped that all the roots to the characteristic equation are real.

There is a third possible motion which is a borderline case. If two roots are real and equal, the system is said to be critically damped. The motion will be aperiodic and both roots will give the same motion.

The general solution to the motion of the system is a linear combination of all the motions defined by the roots to the characteristic equation. Associated with each root is a mode shape which gives the relative amplitudes of each degree of freedom when the system is responding to one particular root. It is of interest to establish these mode shapes so that each stability curve can be associated with a definite motion of the whole system. For example, one mode shape may show that the pitching motion of the balloon is very large compared to the motion of the tether.

C. STABILITY ANALYSIS

Derivations of the equations of motion of the tethered balloon system and development of the characteristic equations for a tethered balloon system approximated with a three-link tether are given in Reference 2.

The four linearized longitudinal equations are Laplace transformed, and an eighth order characteristic equation generated which specifies stability characteristics of the system. In like manner, the five linearized lateral equations can be reduced to a tenth order equation which gives stability information in the lateral degrees-of-freedom. The roots of these characteristic equations identify the natural frequencies, damped frequencies and damping ratios.

D. DYNAMIC RESPONSE ANALYSIS

The calculations of the balloon system response to specific disturbances is the subject of the dynamic response analysis. The most general motion the system can have is a linear superposition of the normal modes.

Each aperiodic or non-oscillatory normal mode has one arbitrary constant (the initial value of any one of the variables) associated with it; and each periodic or oscillatory normal mode has two arbitrary constants (the amplitude and phase angle of any one of the variables) associated with it. The total number of arbitrary constants is then equal to the number of aperiodic modes plus twice the number of periodic modes; i.e. to the degree of the characteristic equation, or the order of the system. A specific disturbance will excite the normal modes in varying degrees and establish the values of the arbitary constants.

The dynamic response of tethered balloon systems to various wind disturbances is obtained by integrating numerically the longitudinal and lateral equations of motion to produce a time history of the dynamics. The start conditions, or equilibrium conditions for the dynamic response computer programs are obtained from the linearized stability computer programs (Reference 2). This approach to analysis has the advantage that wind gusts can be produced and the actual motion of the system can be observed. The major disadvantage is that a greater amount of computer time is required when compared to evaluation of stability by investigating the roots of the characteristic equations.

The equations of motion for the longitudinal dynamics of a tethered balloon system were initially derived in two forms (see Reference 3):

(1) inertia terms which contain products of angular velocities are neglected,

(2) inertia terms which contain products of angular velocities are included.

The concept of neglecting products of angular velocities is associated with the assumption that angular velocities are small; and therefore, products of angular velocities are negligible.

Numerical integrations were made with the computer to determine the effect of neglecting the inertia terms containing products of angular velocities. Although an effect is obviously present, the overall differences between the results of the two sets of equations is small as shown in Reference 3.

It was decided that dynamic simulation studies would be conducted with a model which neglects products of angular velocities for three reasons. First, the equations containing products of angular velocities are shown to give only slightly different results. Second, it is desirable to keep the dynamic equations compatible to the equations used in the stability study (the stability study used linearized equations). Third, it is desirable to keep the longitudinal equations compatible to the lateral equations (to derive the lateral equations of motion containing products of angular velocities in the inertia terms would be a very difficult task because of the number of terms involved.)

SECTION III

TEST BALLOON DESCRIPTION

A. GENERAL

The tethered balloon system which was flown to obtain experimental motion data consisted of a 70,000 cubic foot aerodynamically shaped balloon produced by Lea Bridge Industries of Essex, England, and a Nolaro tether. The Nolaro tether was 0.52 inches in diameter and weighed 90 pounds per 1000 feet. The winch used is permanently installed at Fair Site in the northwestern portion of the White Sands Missile Range.

The general arrangement of the 70,000 cubic foot aerodynamically shaped balloon is presented in Figure 4. The major elements of the balloon are the envelope, the tails and the suspension system. The envelope is divided into three separate chambers - the gas chamber, ballonet, and tail cone. The two near horizontal surfaces and the vertical rudder make up the tails (Table I lists the dimensions for the balloon).

TABLE I

DIMENSIONS FOR THE 70,000 FT^3 KITE BALLOON

PRINCIPAL PARTICULARS

Maximum Capacity of Envelope	70,000 Ft^3
Maximum Volume of Air Filled Tail (lower only)	6,000 Ft^3
Maximum Volume of Horizontal Tails (each)	3,070 Ft^3
Maximum Diameter of Envelope	39 Ft
Length of Envelope	106 Ft 6 In
Overall Width with Fins Inflated	43 Ft
Overall Height from Bottom of Rudder	48 Ft 6 In
Height of Balloon from Rigging Confluence Point	66 Ft
Ballonet Capacity	To permit a flying altitude of 15,000 Ft
Bridle Confluence Point	32 Ft aft of Nose of Hull
	45 Ft below Centerline of Hull

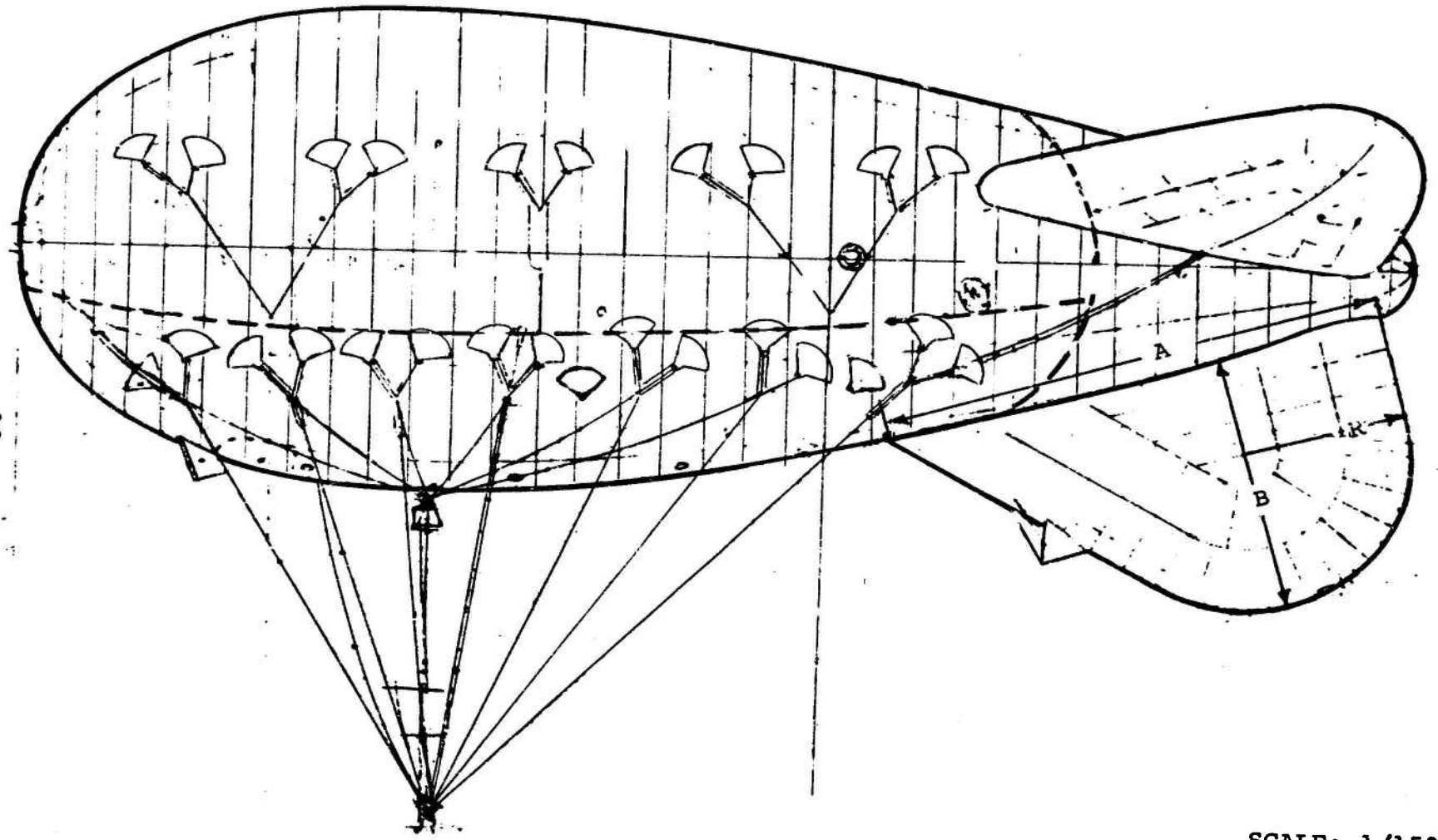

SCALE: 1/150TH.

Figure 4. General Arrangement of 70,000 Cubic Foot Kite Balloon

B. TEST BALLOON GEOMETRY

The geometry of the 70,000 cubic foot balloon was established with the aid of data from the balloon handbook (Reference 4) and the data on the BJ balloon (Reference 5). The overall length and diameter of the hull and location of the confluence point of the suspension lines are listed in Table I. The geometry of tails was established on the basis of data in References 4 and 5.

The pertinent tail dimensions for the tail surfaces are the chord (A), the span (B) and the radius of the tip (R) as defined on Figure 4. From Reference 5 for a BJ balloon, the proportions for the rudder (vertical tail surface) relative to the total envelope length (L) are

$$A = 0.41\ L$$
$$B = 0.23\ L$$
$$R = 0.135\ L$$

All horizontal fin surface dimensions are 80% of rudder dimensions. It is understood that the tail surfaces are as used on the BJ balloon. The test balloon has a hull known as the A shape and this hull has a fineness ratio of 2.7 as compared to 2.5 for the BJ balloon. Consequently, for equal hull volume the test balloon hull is longer than the BJ balloon hull. Tail dimensions for the 70,000 cubic foot barrage balloon were calculated by proportioning the length of an equivalent volume BJ balloon. The rudder dimensions computed for the test balloon are:

$$A = 40 \text{ feet}$$
$$B = 22.4 \text{ feet}$$
$$R = 13.15 \text{ feet}$$

C. BALLOON MASS CHARACTERISTICS

1. General

The balloon's physical and apparent mass characteristics are presented in this section and tabulated in Table II . The mass characteristics include the physical mass, additional masses in longitudinal, lateral and vertical translation, the apparent masses in roll, pitch and yaw; physical mass moments of inertia and apparent mass moments of inertia in roll, pitch, and yaw. Calculations include center of gravity, centers of additional mass and dynamic centers in pitch and yaw.

TABLE II

BALLOON MASS CHARACTERISTICS

Balloon Physical Mass - with payload	118.10	slugs
Center of Gravity - with payload - Horizontal	54.44	feet
- Vertical	6.57	feet
Mass Moment of Inertia, with payload - Roll	30207	slug feet^2
- Pitch	149022	slug feet^2
- Yaw	134027	slug feet^2
Product of Inertia - with payload	10391	slug feet^2
Balloon Physical Mass - without payload	114.04	slugs
Center of Gravity - without payload - Horizontal	55.24	feet
- Vertical	5.30	feet
Mass Moment of Inertia - without payload - Roll	24913	slug feet^2
- Pitch	141614	slug feet^2
- Yaw	131895	slug feet^2
Product of Inertia - without payload	7130	slug feet^2
Additional Mass - Longitudinal	22.00	slugs
- Lateral	166.63	slugs
- Vertical	151.58	slugs
Center of Additional Mass, in pitch - horizontal	56.18	feet
- vertical	0.00	feet
Center of Additional Mass, in yaw - horizontal	58.39	feet
- vertical	1.66	feet
Additional Mass Moment of Inertia - roll	31422	slug feet^2
- pitch	123811	slug feet^2
- yaw	132268	slug feet^2
Additional Product of Inertia - in yaw	-8729	slug feet^2
Apparent Mass, Without Payload - roll	182.97	slugs
- pitch	265.62	slugs
- yaw	280.66	slugs
Dynamic Center, Without Payload, in pitch - horizontal	55.78	feet
- vertical	2.28	feet

TABLE II (cont.)

BALLOON MASS CHARACTERISTICS

Dynamic Center, Without Payload, in yaw - horizontal	57.11	feet
- vertical	3.14	feet
Apparent Mass Moment of Inertia, without payload		
- roll	54404	slug ft^2
- pitch	267256	slug ft^2
- yaw	264854	slug ft^2
Apparent Product of Inertia, without payload - in pitch	7525	slug ft^2
- in yaw	-805	slug ft^2
Apparent Mass, with payload - pitch	269.69	slugs
- yaw	284.73	slugs
Dynamic Center, with Payload, in Pitch - horizontal	55.42	feet
- vertical	2.88	feet
Dynamic Center, with Payload, in yaw - horizontal	56.75	feet
- vertical	3.69	feet
Apparent Mass Moment of Inertia, with Payload - pitch	275832	slug ft^2
- yaw	267400	slug ft^2
Apparent Product of Inertia, with Payload - in pitch	11193	slug ft^2
- in yaw	2896	slug ft^2

Notes:
1. Mass is in slugs
2. Horizontal distance is feet aft of theoretical bow
3. Vertical distance is feet below hull $\mathcal{C}_L$
4. Inertia is in slug $feet^2$
5. Balloon physical mass includes internal gas and air

Based on data received from Air Force Cambridge Research Laboratories, the estimated weight breakdown for the balloon system is given in Table III. This breakdown is considered to be representative of the test balloon flown.

The payload includes batteries, instrument package, instrument frame, cable cutter and load cell.

The density of the air and helium for the balloon mass characteristics analysis was based on a temperature of 50°F. Based on this temperature and the reported cable tension (free lift) it was estimated that the balloon was approximately 88% full of helium with approximately 12% air in the ballonets.

2. Additional Mass

The acceleration of the balloon in any of the six degrees of freedom causes aerodynamic forces in addition to the velocity and attitude changes. It has been shown by Lamb (Reference 6) that the derivatives of these acceleration forces have the dimension of mass. For all practical purposes, this additional mass term may be added to the actual mass of the balloon for purposes of calculating forces and responses of the system. References 7 and 8 were also useful in the development of this section.

The additional mass and additional moments of inertia for acceleration in a fluid have been worked out theoretically for a number of ellipsoids of revolution. Figures 5 and 6 show these coefficients plotted against fineness ratio. The added mass is obtained by multiplying these coefficients by the mass of the displaced air. It has been proposed and has become the custom to use (for airships and balloons) values based on the ellipsoid having the same volume and the same length as the hull. In addition, the theoretical longitudinal coefficient of additional mass shown on the curves are increased 50% to allow for the boundary layer which is dragged along with the balloon.

The fineness ratio of the equivalent ellipsoid to the hull must be computed based on equal volumes and equal lengths.

$$\forall = \frac{\pi}{6} d^2 L$$

$$d = \sqrt{\frac{6 \forall}{\pi L}}$$

$$\text{Fineness ratio} = \frac{L}{\sqrt{\frac{6 \forall}{\pi L}}} = \sqrt{\frac{\pi L^3}{6 \forall}}$$

TABLE III

ESTIMATED BALLOON WEIGHT BREAKDOWN

ITEM	WEIGHT-POUNDS
Hull	875
Horizontal Tail	116
Vertical Tail	91
Ballonet	248
Handling Lines	25
Rip Panel	8
Suspension Cables and Fittings	132
Gas Valves	18
Ballonet Blower	12
Pressure Tubing	6
Electric Cables	7
Miscellaneous Hardware	5
Total Balloon Weignt	1543
Payload	131
Total Flight Weight (less tether)	1674

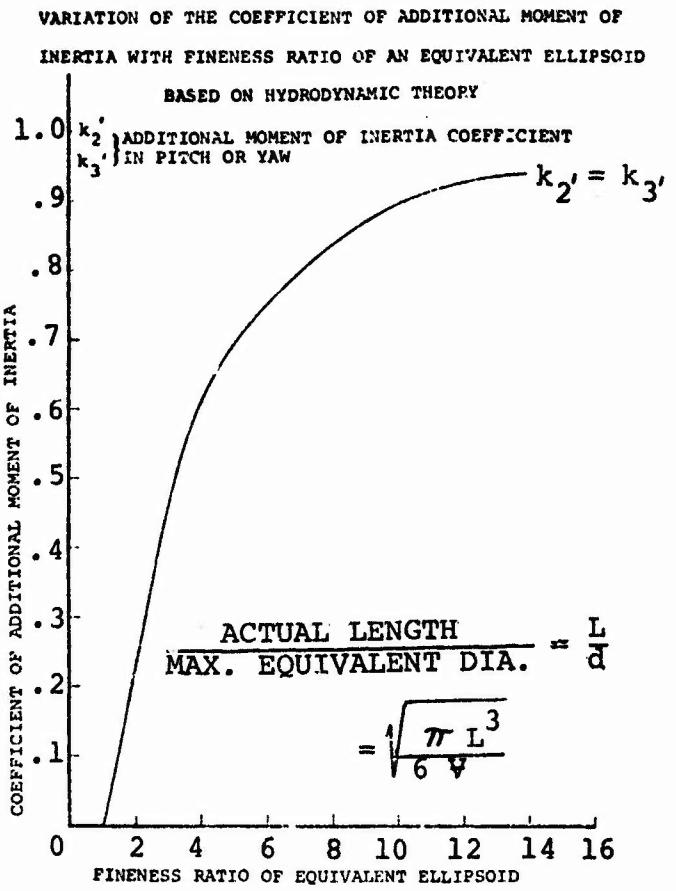

Figure 5. Variation of the Coefficient of Additional Moment of Inertia with Fineness Ratio of an Equivalent Ellipsoid

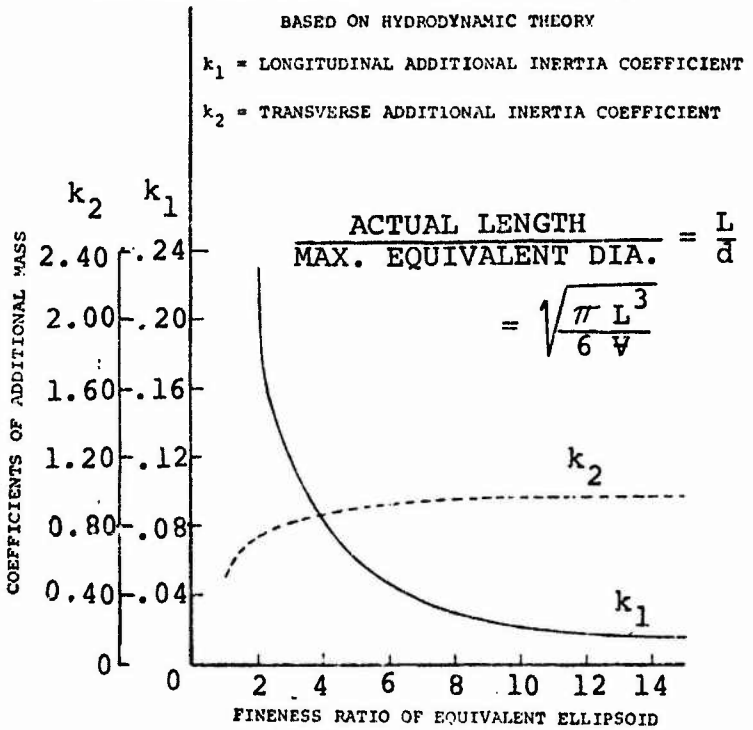

Figure 6. Variation of the Coefficient of Additional Mass with Fineness Ratio of an Equivalent Ellipsoid

The flat tail surfaces also exhibit an added mass effect when accelerated normal to their chords. For large aspect ratios, the added mass is equivalent to the mass of air contained in a cylinder whose diameter is equal to the chord of the tail. Tests have provided corrections for smaller aspect ratios and for taper. The tail added mass terms can be obtained from Figure 7 and added to the hull added mass for the total added mass and moment of inertia effects, and for determining the dynamic center.

The added mass of the tail is obtained by multiplying these coefficients of the mass of air contained in a cylinder having the length equal to the span and a diameter equivalent to the chord of a rectangular tail having the same area.

3. Dynamic Center Location

Under dynamic loads the balloon will have a mass and moment of inertia which includes the additional mass and additional moment of inertia of the affected surrounding air.

Because of symmetry in the XZ plane the only product of inertia considered is P_{XZ}. Since the product of inertia about any axis of symmetry is zero, P_{XY} and P_{YZ} are therefore zero.

The additional mass along each major axis is added directly to the mass of the balloon. The center of the additional mass, however, does not coincide with the center of gravity. The combination of these two masses will determine the dynamic center about which the complete balloon will act in air. Since the value and location of the additional mass is different for accelerations along each axis, the dynamic center will be located at different places for the lateral and vertical accelerations.

Figure 8 shows how the dynamic center is located and the combined moment of inertia is calculated.

D. AERODYNAMIC CHARACTERISTICS

The static aerodynamic characteristics for the test balloon were developed from wind tunnel data obtained at the University of Washington as reported in References 9, 10 and 11. The aerodynamic coefficients as taken from these references are plotted in Figures 9 and 10. Note that the force coefficients are based upon a reference area of hull volume to the two thirds power which is compatible with the equations of motion which have been developed. However, the moment coefficients in Figures 9 and 10 are based upon a reference length of hull length and are about a reference center near the bridle confluence point of the bridle as noted in Figure 10.

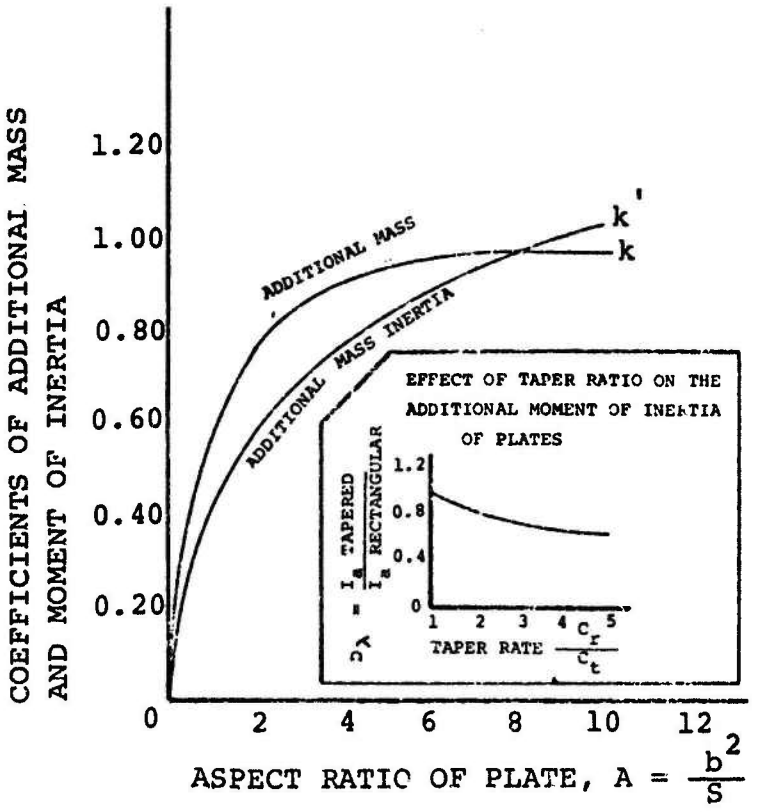

FIGURE 7. VARIATION OF THE COEFFICIENTS OF ADDITIONAL MASS AND MOMENT OF INERTIA WITH ASPECT RATIO OF RECTANGULAR PLATES

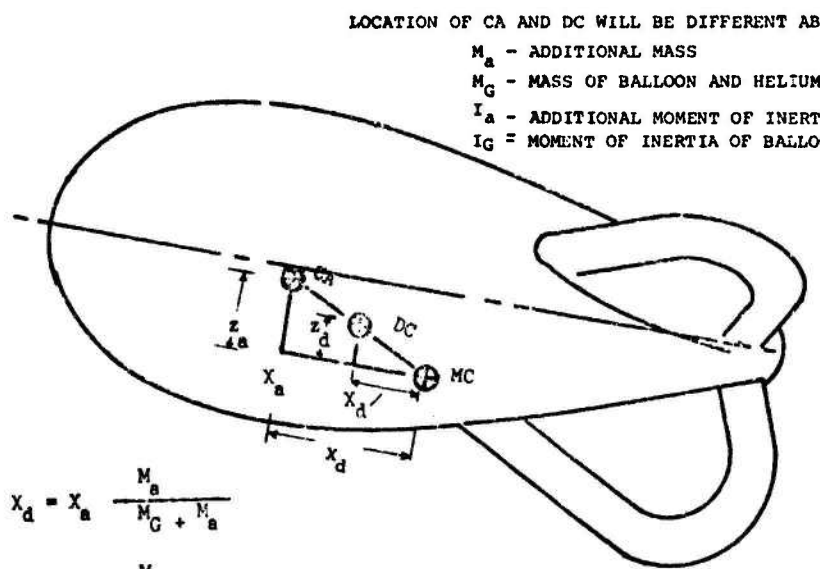

$$X_d = X_a \frac{M_a}{M_G + M_a}$$

$$z_d = z_a \frac{M_a}{M_G + M_a}$$

$$I_D = I_G + I_a + M_a \left[(X_a - X_d)^2 + (z_a - z_d)^2 \right] + M_G \left[X_d^2 + z_d^2 \right]$$

FIGURE 8. LOCATION OF DYNAMIC CENTER (DC) FROM MASS CENTER (MC) AND CENTER OF ADDITIONAL MASS (CA)

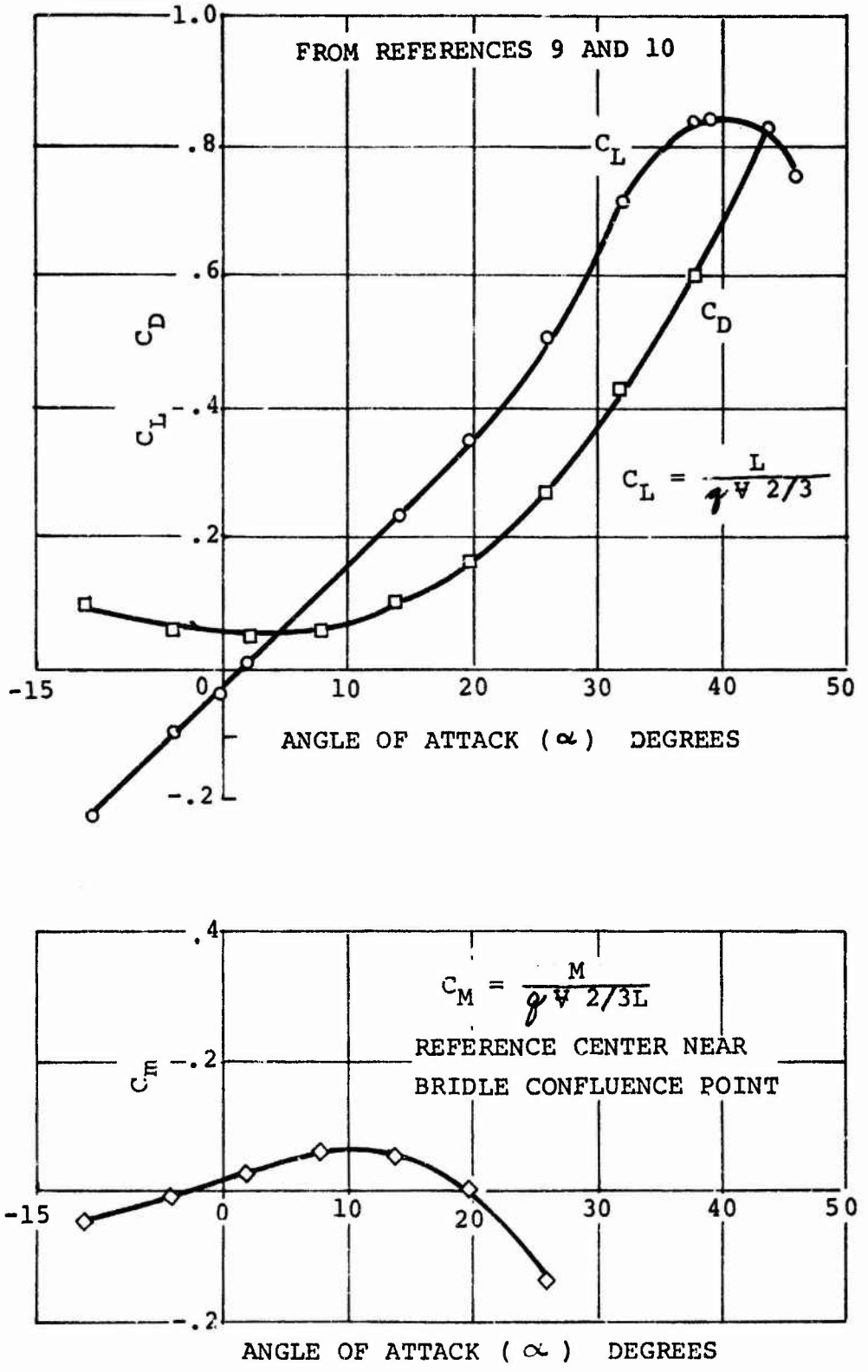

FIGURE 9. LONGITUDINAL STATIC AERODYNAMIC CHARACTERISTICS OF BARRAGE BALLOON

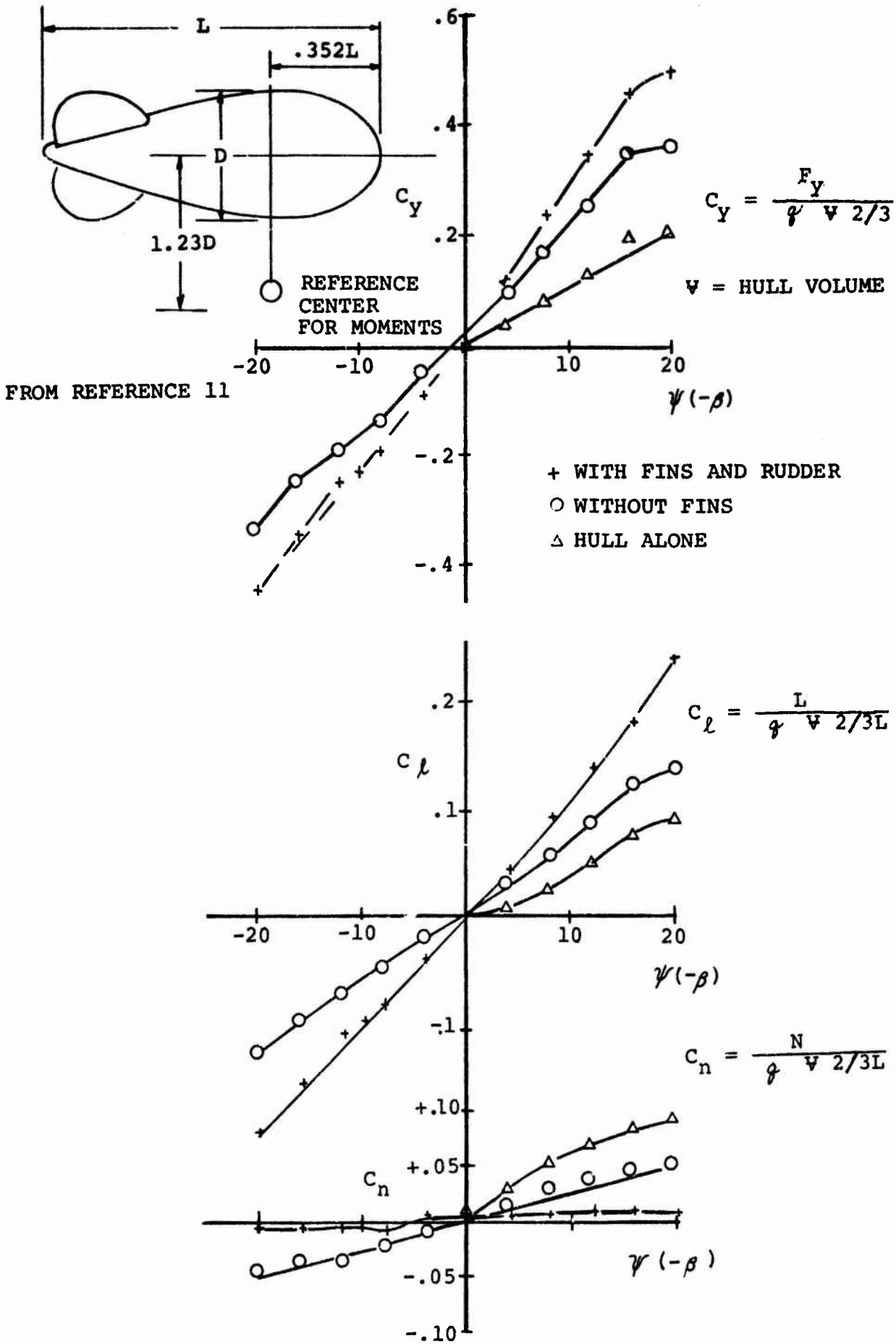

Figure 10. Lateral Static Aerodynamic Characteristics

The static moment coefficients for the test balloon have been adjusted to change the reference length from hull length to $\forall^{1/3}$ and the moments have been transferred from a reference center near the bridle confluence point to the center of volume of the hull. The static aerodynamic coefficients adjusted for reference length and reference center are listed in Tables IV and V.

The dynamic aerodynamic characteristics of the BJ balloon were developed analytically as reported in References 1 and 2. These coefficients were modified for the test balloon by accounting for the longer tail surface moement arms of this configuration. The dynamic coefficients are also listed in Tables IV and V.

TABLE IV

BARRAGE BALLOON LONGITUDINAL AERODYNAMICS

(Moments About Center of Hull Voluma)

(Reference Area $\forall_{Hull}^{2/3}$ - Reference Length $\forall^{1/3}$)

Angle of Attack (α)	-10	-5	0	5	10	15	20	25
Lift Coefficient (C_L)	-.21	-.115	-.02	+.07	+.16	+.255	+.345	+.47
Drag Coefficient (C_D)	.09	.065	.05	.05	.07	.11	.16	.25
Pitching Moment (C_m)	-.280	-.1397	-.0352	+.0595	+.5194	-.069	-.2765	-.713

Lift Force due to Pitch Velocity $C_{L_{\dot{\theta}_B}} = 2.11/\text{rad}$

Pitching Moment Due to Pitch Velocity $C_{m_{\dot{\theta}_B}} = -3.21/\text{rad}$

Drag Force due to Pitch Velocity $C_{D_{\dot{\theta}_B}} = 0.9\, C_L C_{L_{\dot{\theta}_B}}$

TABLE V

BARRAGE BALLOON LATERAL AERODYNAMICS

(Moments About Center of Hull Volume)

(Reference Area $\forall_{Hull}^{2/3}$ - Reference Length $\forall^{1/3}$)

Static Aerodynamic Coefficients

Sideslip Angle (β)	-20	0	+20
Side Force Coefficient (C_y)	+.450	0.0	-.450
Yaw Moment Coefficient (C_n)	+.0787	0.0	-.0787
Roll Moment Coefficient (C_ℓ)	-.008	0.0	+.008

Dynamic Aerodynamic Coefficients

Side Force Due to Yaw Velocity	$(C_{y_{\dot{\psi}_B}})$	+2.19/Rad
Yaw Moment Due to Yaw Velocity	$(C_{n_{\dot{\psi}_B}})$	-3.49/Rad
Roll Moment Due to Yaw Velocity	$(C_{\ell_{\dot{\psi}_B}})$	- .442/Rad
Side Force Due to Roll Velocity	$(C_{y_{\dot{\phi}_B}})$	+ .142/Rad
Yaw Moment Due to Roll Velocity	$(C_{n_{\dot{\phi}_B}})$	- .170/Rad
Roll Moment Due to Roll Velocity	$(C_{\ell_{\dot{\phi}_B}})$	- .327/Rad

Static Aerodynamic Stability Derivatives

Side Force Due to Yaw Angle	$(C_{y_{\psi_B}})$	+1.29/Rad
Side Force Due to Lateral Velocity	$(C_{y_{v_B}})$	-1.29/Rad
Yaw Moment Due to Yaw Angle	$(C_{n_{\psi_B}})$	+ .226/Rad
Yaw Moment Due to Lateral Velocity	$(C_{n_{v_B}})$	- .226/Rad
Roll Moment Due to Yaw Angle	$(C_{\ell_{\psi_B}})$	- .0229/Rad
Roll Moment Due to Lateral Velocity	$(C_{\ell_{v_B}})$	+ .0229/Rad

SECTION IV

FLIGHT TEST PROCEDURES

Flight tests were conducted to obtain experimental balloon motion data for comparison with analytical predictions. As stated previously, a 70,000 cubic foot barrage balloon and a 0.52 inch diameter Nolara tether were flown.

Instrumentation consisted of the following items:

(a) Cinetheodolite coverage of balloon to obtain X, Y and Z coordinates of the balloon. Motion was measured at the confluence point of balloon suspension lines.

(b) Motion picture coverage of balloon motion (camera looked up vertically from tether point to give balloon yawing motion).

(c) A telemetry package located at the confluence point which provided

  (1) Horizontal relative wind speed

  (2) Vertical relative wind speed

  (3) X, Y and Z acceleration

  (4) Roll angle

  (5) Pitch angle

  (6) Ambient pressure

  (7) Differential pressure (helium compartment)

(d) Pilot balloon data which gives wind direction and magnitude.

Five flight test data runs were made. The balloon was displaced and then released to obtain motion of the tethered balloon system. The balloon was pulled to the side to excite lateral motions and was pulled aft to excite longitudinal motion. A light nylon line attached to the confluence point of the balloon suspension lines provided initial displacement of the balloon. The line was secured at the ground a known distance from the ground tether point. The tether cable was then payed out until tether tension was re-

duced to one half. A test was initiated by cutting the auxiliary line at the ground.

The above listed data items were recorded for the following test conditions.

(a) Run #1 - Lateral balloon displacement of 100 feet to right. Tether length - 1079 feet.

(b) Run #2 - Longitudinal balloon displacement of 150 feet aft. Tether length - 1118 feet.

(c) Run #3 - Lateral balloon displacement of 150 feet to right. Tether length - 1066 feet.

(d) Run #4 - Lateral balloon displacement of 150 feet to right. Tether length - 663 feet.

(e) Run #5 - Longitudinal balloon displacement of 150 feet aft. Tether length - 684 feet.

Table VI presents the test log for the flight test program.

TABLE VI - TETHERED BALLOON FLIGHT TEST LOG, NOVEMBER 10, 1972

Test Item - 70,000 Cubic Foot Kite Balloon-Nolara Tether .52 Inch Diameter, 90 Pounds/ 1000 Feet Otis Winch Installed at Fairsite

Run #1 - Lateral Disturbance
Tether Cable Length - 1079 Ft.
Balloon Displacement-
100 ft to right of
Equilibrium Position
Balloon Release Time - 12:00
Tension at Winch -
Initial before release - 500lbs
Fluctuation after release -
1300-1500 lbs.

Pilot Balloon Data - 12:00

Alt. (Ft.)	Wind Direction (True) (Degrees)	Wind Speed (Knots)
Ground	185	05
300	190	07
600	190	09
900	190	11
1200	190	12
1500	190	12
1800	190	12
2100	190	13

Run #2 - Longitudinal Disturbance
Tether Cable Length - 1118 Ft.
Balloon Displacement -
150 Ft. Back of
Equilibrium Position
Balloon Release Time - 12:32
Tension at Winch
Initial before Release - 600lbs
Fluctuation after release -
1350-1450 lbs.

Pilot Balloon Data - 12:40

Alt. (Ft.)	Wind Direction (True) (Degrees)	Wind Speed (Knots)
Ground	120	04
300	130	04
600	150	04
900	155	04
1200	160	05
1500	175	07
1800	180	08
2100	195	09

TABLE VI - TETHERED BALLOON FLIGHT TEST LOG, NOVEMBER 10, 1972 (cont.)

Run #3 - Lateral Disturbance
Tether Cable Length - 1086 Ft.
Balloon Displacement - 150 Ft. to right
Balloon Release time - 1:05 PM
Tension at Winch
Initial Before Release - 600 lbs
Immediate Peak After Cut - 1300 lbs
Fluctuation After Release - 1200-1700 lbs

Run #4 - Lateral Disturbance
Tether Cable Length - 663 Ft.
Balloon Displacement -
150 Ft. to right
Balloon Release Time - 1:40 pm
Tension at Winch
Initial Before Release -
800 lbs.
Immediate Peak After Cut -
1400 lbs.
Fluctuation After Release -
1150-1250 lbs.

Pilot Balloon Data - 1:38 pm

Alt. (Ft.)	Wind Direction (True) (Degrees)	Wind Speed (Knots)
Ground	190	03
300	185	04
600	180	06
900	175	07
1200	175	09
1500	175	09
1800	180	10
2100	185	11

TABLE VI - TETHERED BALLOON FLIGHT TEST LOG, NOVEMBER 10, 1972 (cont.)

Run #5 - Longitudinal Disturbance
Tether Cable Length - 684 Ft.
Balloon Displacement -
150 Ft. Back
Balloon Release Time - 2:12 pm
Tension at Winch
Initial Before Release -
600 lbs.
Immediate Peak After Cut -
1800 lbs.
Fluctuation After Release -
1000-1100 lbs.

Pilot Balloon Data - 2:10 pm

Alt. (Ft.)	Wind Direction (True) (Degrees)	Wind Speed (Knots)
Ground	230	01
300	225	02
600	210	04
900	195	05
1200	190	06
1500	190	06
1800	190	07
2100	185	07

Conditions After Test

Tether Cable Length - 0 Ft.
Time - 3:07 pm
Tether Tension -1250lbs Steady

Pilot Balloon Data - 3:08 pm

Alt. (Ft.)	Wind Direction (True) (Degrees)	Wind Speed (Knots)
Ground	130	03
300	130	04
600	130	05
900	135	05
1200	135	06
1500	145	07
1800	150	07
2100	155	08

SECTION V

COMPARISON OF EXPERIMENTAL AND ANALYTICALLY PREDICTED DYNAMIC BEHAVIOR OF TETHERED BALLOONS

A. GENERAL

The geometric, mass and aerodynamic characteristics of the tethered balloon system which was flown have been described earlier in this report. The characteristic equations for longitudinal and lateral motion were solved to establish predicted natural frequencies, damped frequencies and damping ratios for this system. The dynamic response of the tethered balloon system to disturbances simulating test conditions was obtained by numerically integrating the longitudinal and the lateral equations of motion.

Initial conditions of displacement and tension were put into the dynamic simulation program as estimated from flight test data for a given test case. During tests, an auxiliary load was applied by the control line at the bridle confluence point to obtain initial balloon displacement aft or to the right. For computations, the balloon was displaced as in tests and the reduced tether tension as a result of the auxiliary load was simulated by an artificial payload which is removed at time one second of the calculations.

Computations were made with the stability and dynamic simulation computer programs to establish the predicted dynamic behavior of this balloon for two test conditions.

> Longitudinal Test Run No. 5 was chosen for analysis because test data indicated relatively little lateral motion.
>
> Test Run No. 3 was chosen for the lateral motion test since this test had the largest initial lateral displacement and data was available over the greatest length of time.

A comparison and correlation of analytically predicted and experimentally determined dynamic response for the tethered balloon system is discussed herein.

B. LONGITUDINAL MOTION

Calculated dynamic behavior of the barrage balloon for Longitudinal Test Run No. 5 is plotted in Figures 11a, 11b and 11c. An estimated wind speed of 17.4 feet per second was obtained from the onboard cup anemometer telemetry record (i.e., prior to release of the balloon).

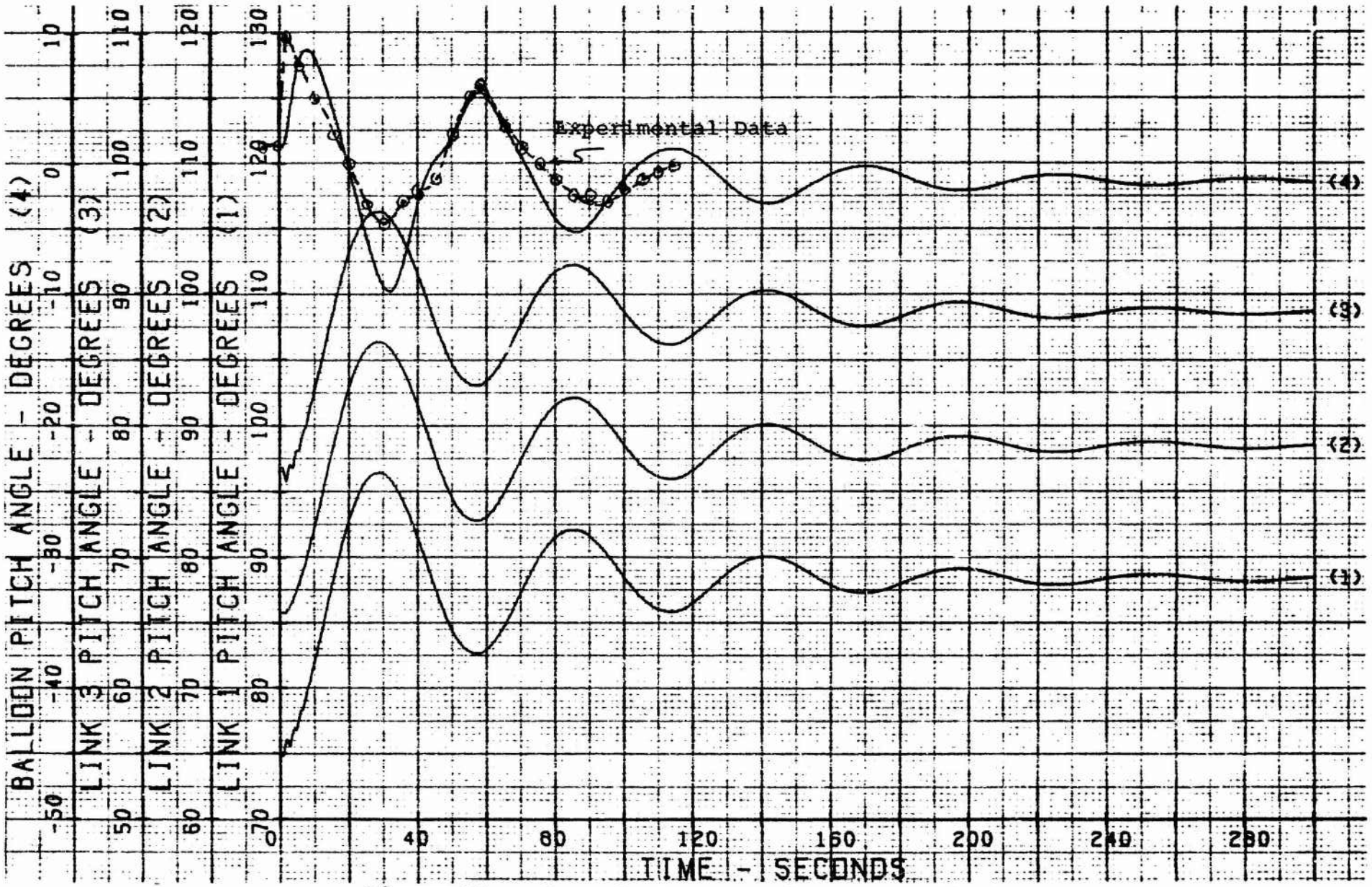

Figure 11a. Dynamic Response for Longitudinal Test Run No. 5

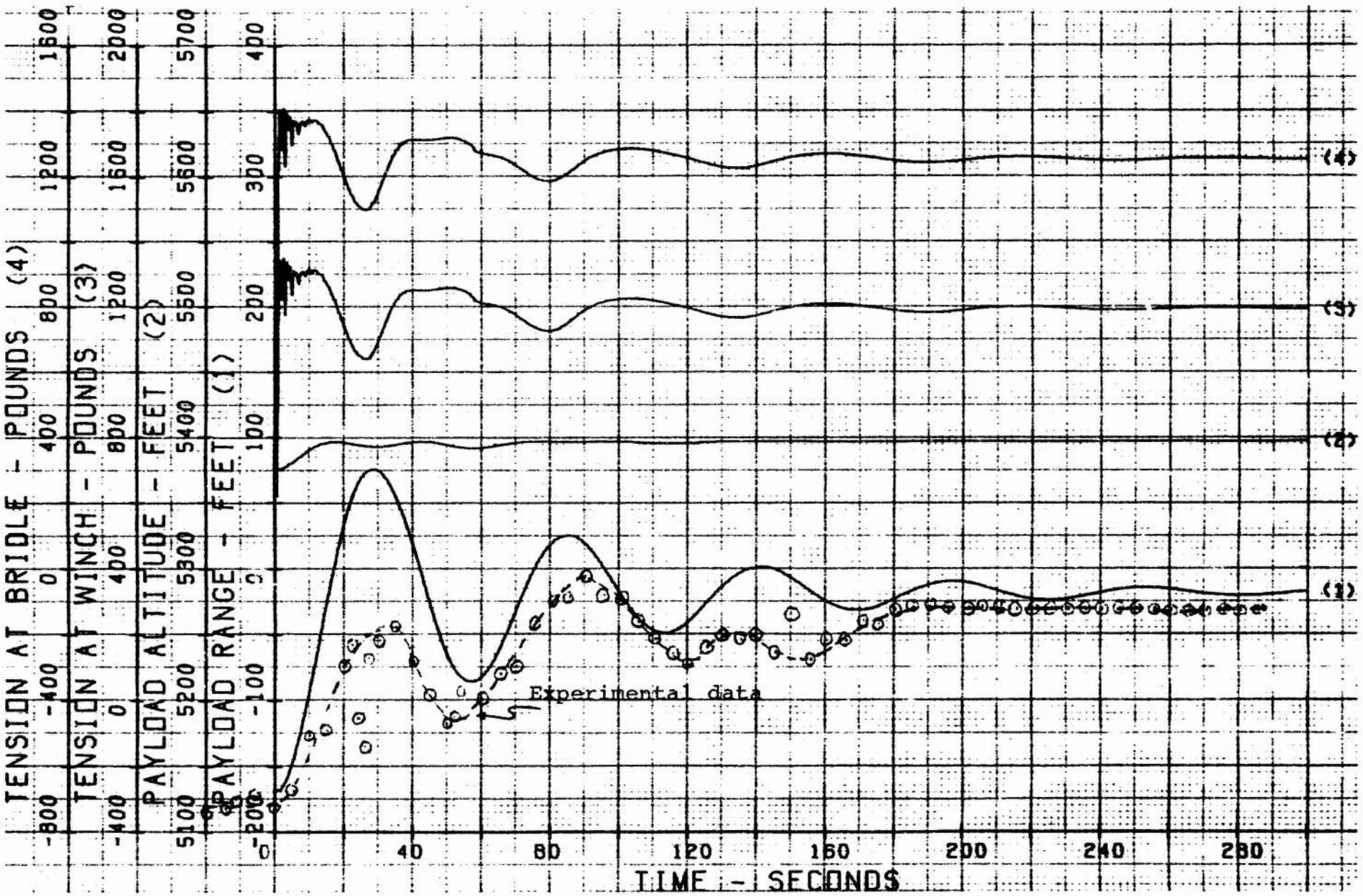

Figure 11b. Dynamic Response for Longitudinal Test Run No. 5

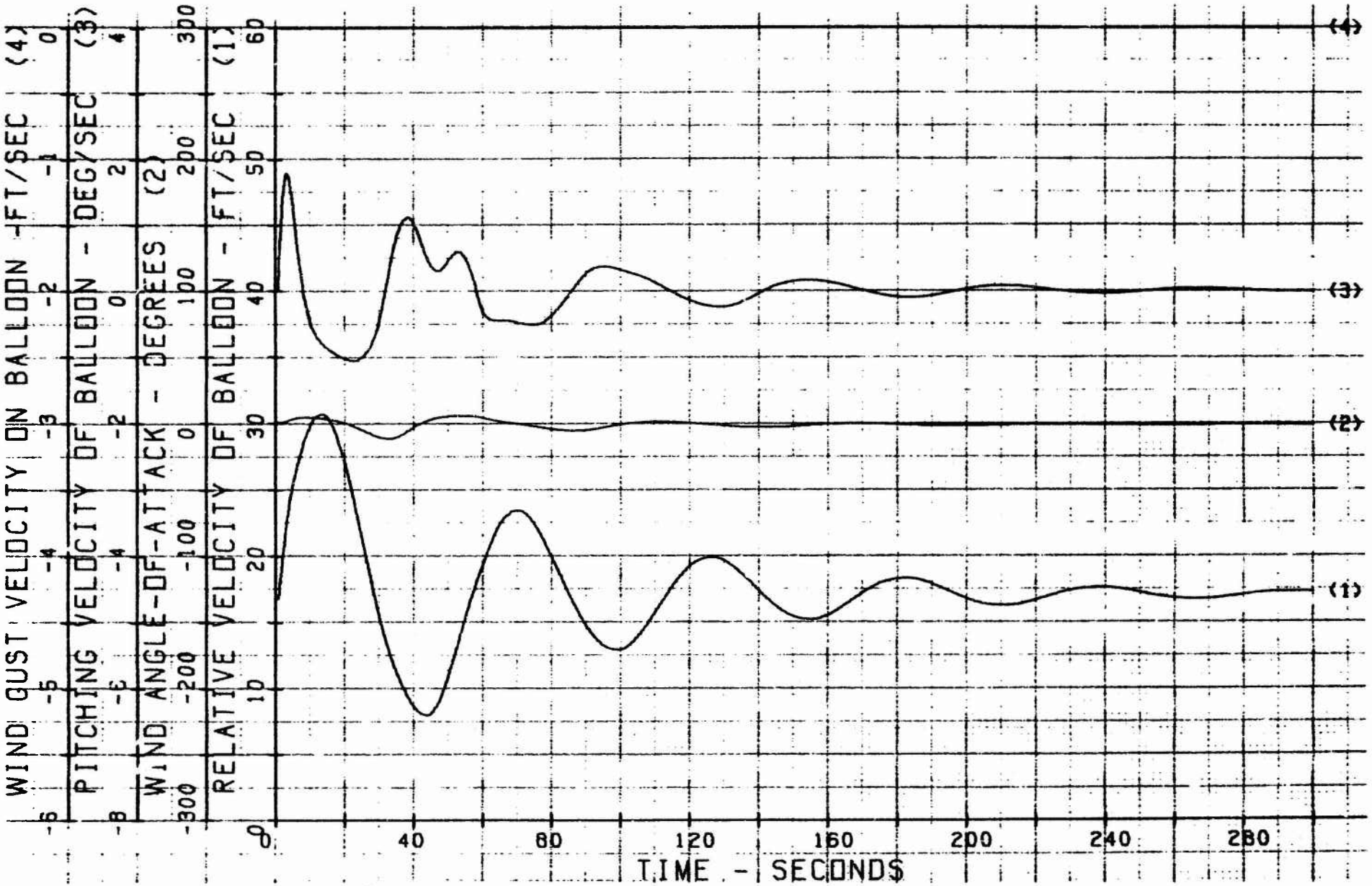

Figure 11c. Dynamic Response for Longitudinal Test Run No. 5

Pilot balloon wind data was ratioed to this value to obtain the estimated wind on the tether. Balloon pitch angle and fore and aft motion as measured during the tests are superimposed on these plots for comparison purposes. Correlation of pitch angle appears good. The frequency of motion is comparable and damping during the test is somewhat greater. Initial measured pitching motion may be attributable to instrumentation package motion rather than the balloon itself. Stability data is listed in Table VII for this case. The first computed mode of motion is a damped mode which has a damped frequency of .1132 rad/sec. Referring to the mode shapes of Table VII this represents a motion where the cable links move as a unit and balloon pitching motion is approximately 180 degrees out of phase. This phase relationship is also apparent in Figure 11a where the three links comprising the tether move together and the balloon pitch angle is 180 degrees out of phase. The experimental results indicate a pitching frequency of 0.10 rad/sec which is in reasonable agreement.

Again referring to Figure 11b, the frequency of fore and aft motion (payload range) shows that reasonable agreement exists between experiment and predictions. Experimental motion is more highly damped. Although motion is primarily in the longitudinal plane, some yawing of the balloon did occur during the experiment, as shown in Figure 12. This would increase aerodynamic drag and some of the additional damping might be attributed to this. Also, all damping coefficients used in the theoretical predictions were calculated for zero angle-of-attack and zero side slip angle. It is apparent that the first mode of motion is the dominant one which has been excited.

C. LATERAL MOTION

Predicted dynamic behavior of the tethered balloon system for Lateral Test Run No. 3 is plotted in Figures 13a, 13b and 13c. Wind data used for the computer simulation was based on telemetry data from the cup anemometer before release of the balloon. The lateral displacement (payload cross range) comparison between prediction and experiment shows obvious discrepancies (Figure 13a). Initial lateral displacement is similar but as time progresses the balloon actually begins to converge to a different equilibrium position and some forcing function causes the balloon to oscillate with relatively high amplitude.

The stability analysis for Lateral Test Run No. 3 is listed in Tables VIII and IX. Referring to Table VIII, the first mode of motion has the following characteristics:

Table VII. STABILITY ANALYSIS OF A TETHERED BALLOON IN THE LONGITUDINAL PLANE CASE 5 BJ BALLOON(A SHAPE) 70000. CU

ALTITUDE PROFILE	0.0	4713.0	5013.0	5313.0	5613.0	5913.0	6300.0	0.0
WIND VELOCITY PROFILE	4.0	4.0	8.0	16.0	20.0	24.0	24.0	0.0

ANGLE-OF-ATTACK(DEG)	-10.0000	-5.0000	0.0	5.0000	10.0000	15.0000	20.0000	25.0000
MOMENT COEFFICIENT	-0.2800	-0.1397	-0.0352	0.0595	0.5194	-0.0690	-0.2765	-0.7130
LIFT COEFFICIENT	-0.2100	-0.1150	-0.0200	0.0700	0.1600	0.2550	0.3450	0.4700
DRAG COEFFICIENT	0.0900	0.0650	0.0500	0.0500	0.0700	0.1100	0.1600	0.2500

DELTA	XIO(1)	XIO(2)	XIO(3)
1.00000	87.99995	88.99994	89.49997
-1.35722	88.43430	88.49042	88.59712
-1.40771	88.42931	88.48637	88.59341
-1.40386	88.43015	88.48669	88.59373
-1.40415	88.43015	88.48669	88.59373
-1.40420	88.43015	88.48669	88.59373
-1.40415	88.43015	88.48669	88.59373
-1.40420	88.43015	88.48665	88.59373
-1.40415	88.43015	88.48665	88.59373
-1.40409	88.43015	88.48669	88.59373
FINAL SOLUTION			
-1.40415	88.43015	88.48669	88.59373

RJM	RKM	CMB	CMAB	CMTDB	LS	MPL	TETH	IX3
RJA	RKA	CLB	CLAB	CLTDB	WB	SB	DC	MAL
RJC	RKC	CDB	CDAB	CDTDB	WTC	DB	CDC	MAV
RJB	RKB	RANGE	ALTITUDE	DYPRB				
23.4200	-43.6200	-0.0845	1.1975	-3.2100	5080.	4.09	684.	357404.
9.7000	-46.5000	-0.0957	1.0886	2.1100	3668.0	1700.0	0.0434	22.00
23.2400	-41.2000	0.0947	-0.1719	-0.0866	61.5	41.200	1.100	151.500
17.200	-45.690	-40.1	5438.5	0.316E 00				

ALPHA(I,J)

0.76E 06	-0.14E 07	-0.14E 07	-0.14E 07
-0.14E 07	0.74E 07	0.74E 07	0.73E 07
-0.14E 07	0.74E 07	0.73E 07	0.73E 07
-0.14E 07	0.73E 07	0.73E 07	0.73E 07

BETA(I,J)

0.19E 06	-0.38E 04	-0.38E 04	-0.38E 04
-0.74E 05	0.21E 06	0.20E 06	0.18E 06
-0.73E 05	0.20E 06	0.20E 06	0.13E 06
-0.72E 05	0.16E 06	0.18E 06	0.18E 06

GAMMA(I,J)

0.63E 05	0.0	0.0	0.0
-0.25E 05	0.27E 06	0.12E 02	0.28E 02
-0.25E 05	0.0	0.28E 06	0.29E 02
-0.24E 05	0.0	0.0	0.28E 06

COEFFICIENTS OF CHARACTERISTIC EQUATION IN ASCENDING ORDER

0.1370 22 0.7060 22 0.1250 24 0.3460 24 0.860D 24 0.687D 23 0.995D 23 0.146D 22 0.1630 22

ALL ROOTS HAVE BEEN ACCURATELY DETERMINED

ROOTS OF CHARACTERISTIC EQUATION REAL	ROOTS OF CHARACTERISTIC EQUATION IMAGINARY	STABILITY PARAMETERS NATURAL FREQUENCY	STABILITY PARAMETERS DAMPED FREQUENCY	STABILITY PARAMETERS DAMPING RATIO	TIME TO HALF OR DOUBLE AMPLITUDE
-0.19100 00	0.30010 00	0.3557D 00	0.3001D 00	0.5369D 00	0.3623D 01
-0.19100 00	-0.30010 00	0.3557D 00	0.3001D 00	0.5369D 00	0.3623D 01
-0.1365D-01	-0.11320 00	0.1140D 00	0.1132D 00	0.1198D 00	0.5077D 02
-0.1365D-01	0.11320 00	0.1140D 00	0.1132D 00	0.1198D 00	0.5077D 02
-0.15200 00	0.31790 01	0.3183D 01	0.3179D 01	0.4776D-01	0.4563D 01
-0.15200 00	-0.31790 01	0.3183D 01	0.3179D 01	0.4776D-01	0.4563D 01

Table VII (Cont)

-0.9270D-01	-0.7112D 01	0.7113D 01	0.7112D 01	0.1303D-01	0.7477D 01
-0.9270D-01	0.7112D 01	0.7113D 01	0.7112D 01	0.1303D-01	0.7477D 01

MODE SHAPES

EIGENVECTORS

REAL	IMAGINARY	MAGNITUDE	DIRECTION ANGLE
0.6248E-01	-0.1703E-02	0.6290E-01	0.3584E 03
0.6119E-01	-0.1972E-02	0.6122E-01	0.3582E 03
0.5853E-01	-0.1761E-02	0.5853E-01	0.3583E 03
0.6274E-01	0.1703E-02	0.6290E-01	0.1551E 01
0.6119E-01	0.1972E-02	0.6122E-01	0.1846E 01
0.5850E-01	0.1764E-02	0.5853E-01	0.1725E 01
-0.9903E 00	0.1450E 00	0.1001E 01	0.1717E 03
-0.9716E 00	0.1461E 00	0.9825E 00	0.1714E 03
-0.9502E 00	0.1550E 00	0.9623E 00	0.1707E 03
-0.9903E 00	-0.1450E 00	0.1001E 01	0.1883E 03
-0.9716E 00	-0.1461E 00	0.9825E 00	0.1896E 03
-0.9502E 00	-0.1550E 00	0.9628E 00	0.1893E 03
-0.1654E 03	-0.2522E 02	0.1665E 03	0.1891E 03
0.2166E 01	0.2708E 01	0.3468E 01	0.5133E 02
0.1632E 03	0.2354E 02	0.1649E 03	0.8208E 01
-0.1644E 03	0.2622E 02	0.1665E 03	0.1709E 03
0.2166E 01	-0.2708E 01	0.3468E 01	0.3087E 03
0.1632E 03	-0.2354E 02	0.1649E 03	0.3518E 03
0.4635E 03	-0.4098E 02	0.4653E 03	0.3549E 03
-0.9293E 03	0.9136E 02	0.9338E 03	0.1744E 03
0.4667E 03	-0.5041E 02	0.4694E 03	0.3538E 03
0.4635E 03	0.4098E 02	0.4653E 03	0.5053E 01
-0.9293E 03	-0.9136E 02	0.9338E 03	0.1855E 03
0.4667E 03	0.5041E 02	0.4694E 03	0.6164E 01

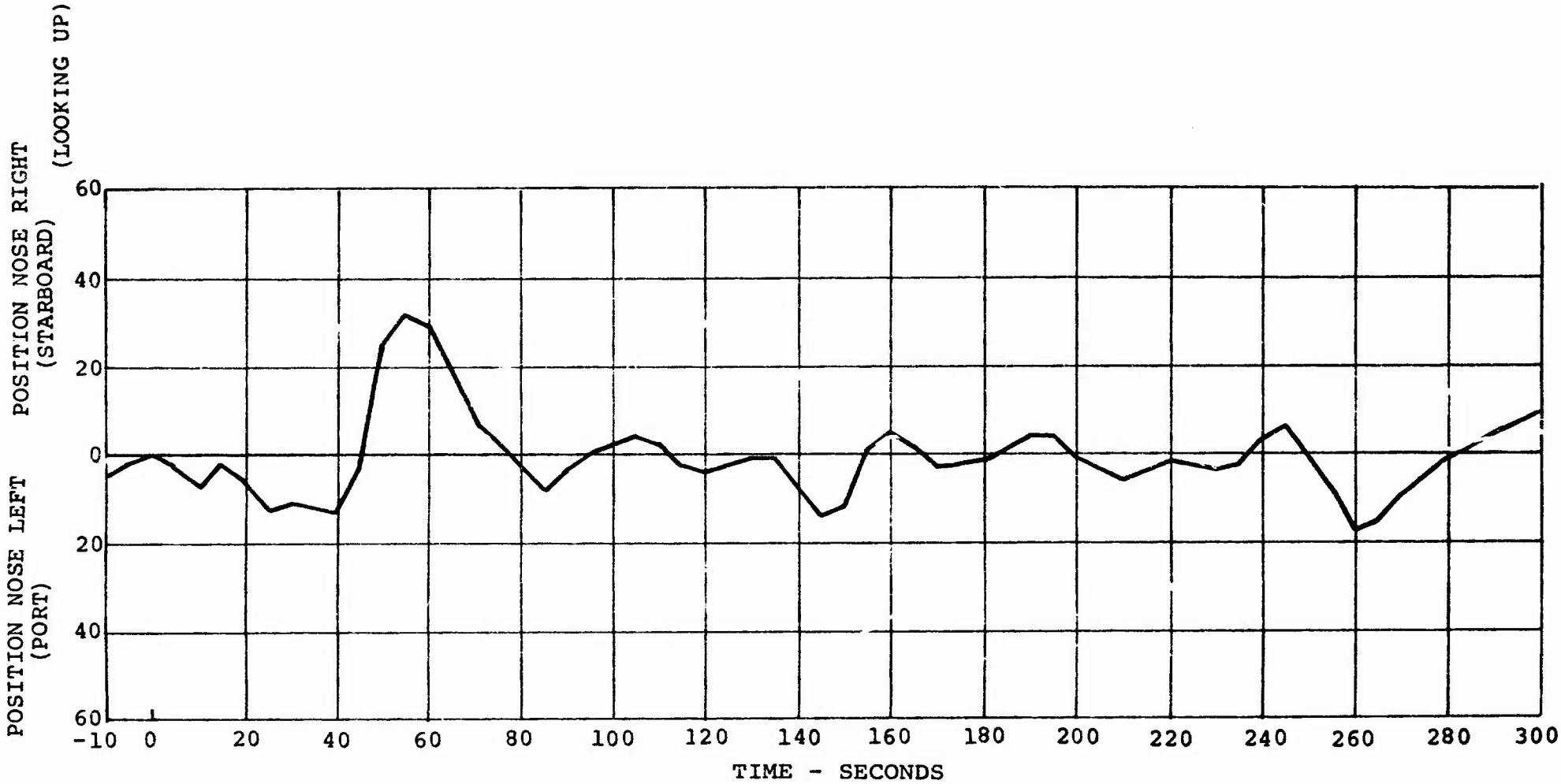

Figure 12. Measured Balloon Yaw Angle for Longitudinal Test Run No. 5

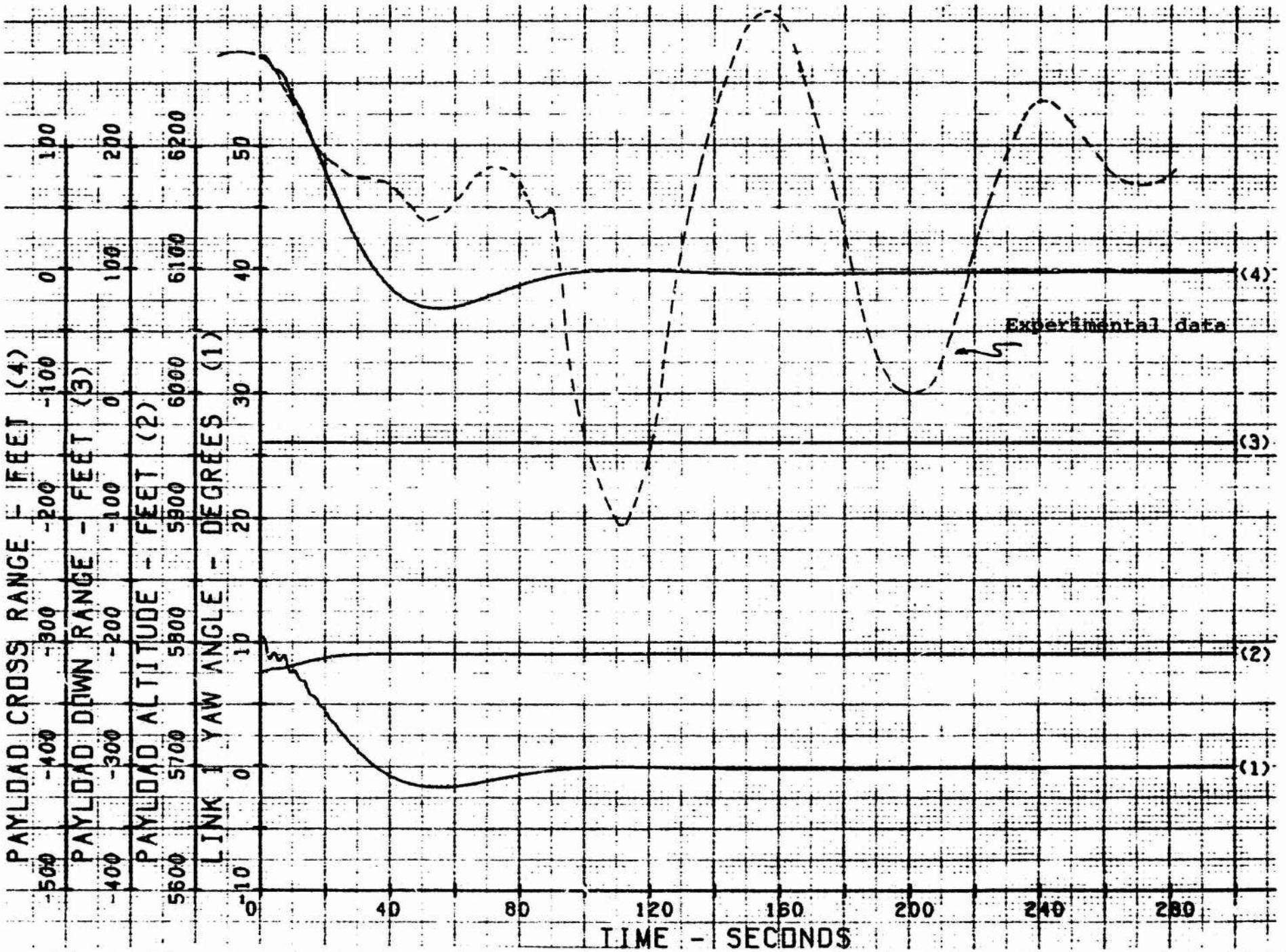

Figure 13a. Dynamic Response for Lateral Test Run No. 3 Initial Balloon Displacement to Right

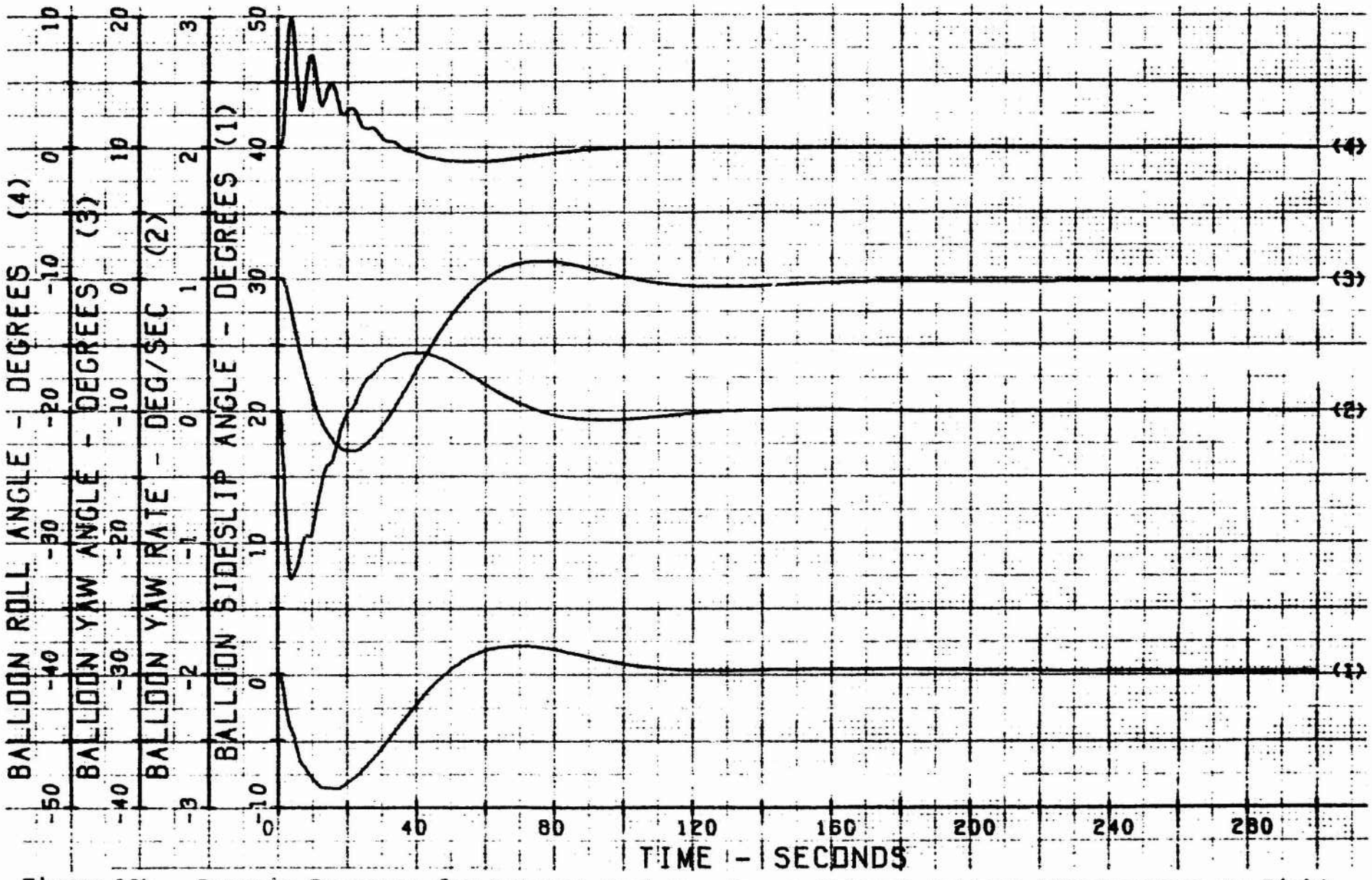

Figure 13b. Dynamic Response for Lateral Test Run No. 3 Initial Balloon Displacement to Right

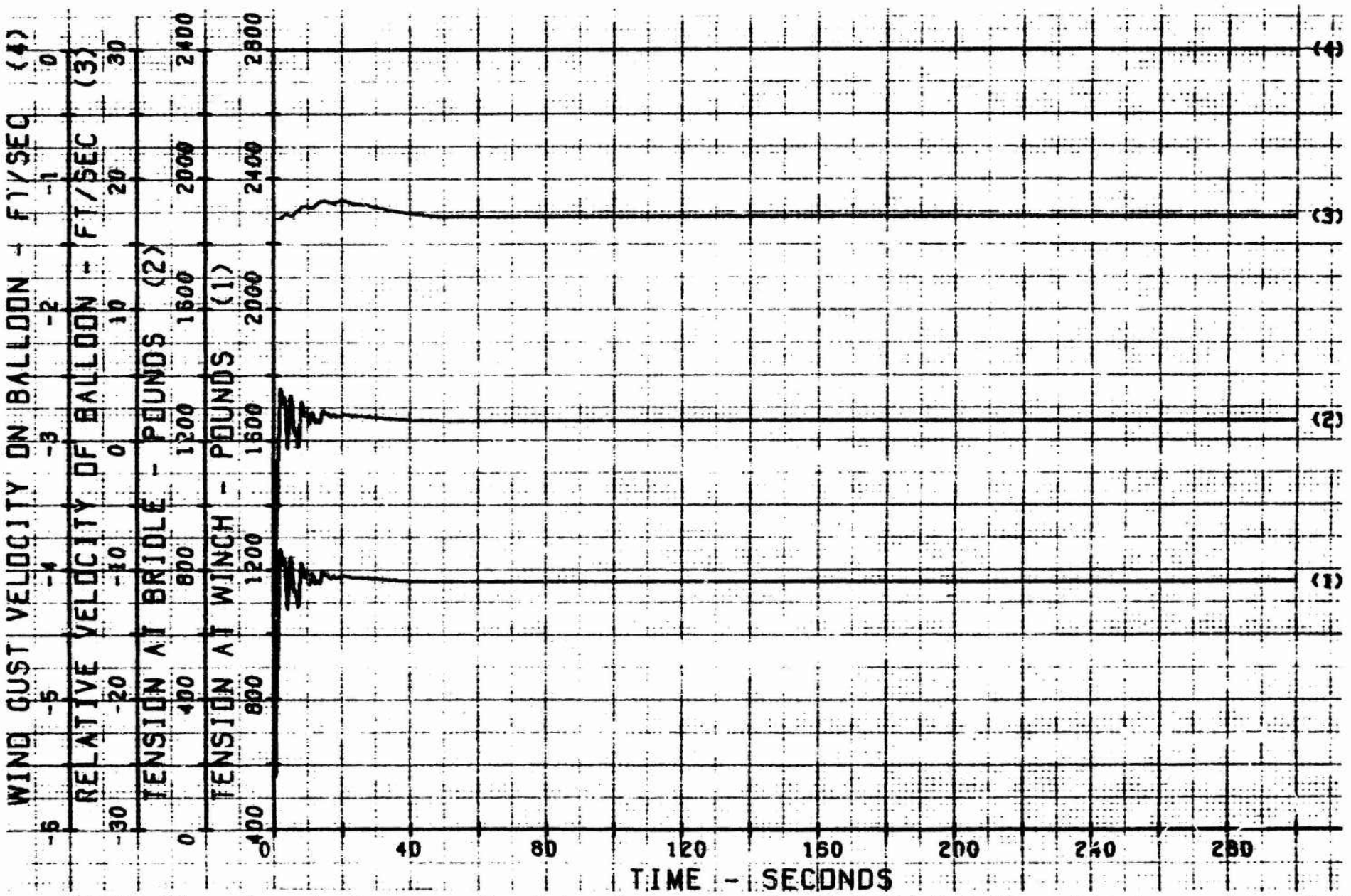

Figure 13c. Dynamic Response for Lateral Test Run No. 3 Initial Balloon Displacement to Right

Table VIII. STABILITY ANALYSIS OF A TETHERED BALLOON IN THE LATERAL PLANE CASE 3 8J BALLOON 70000 CU. FT. 100%

ALTITUDE PROFILE 0.0 4713.0 5013.0 5313.0 5613.0 5913.0 7000.0 0.0
WIND VELOCITY PROFILE 6.0 6.0 8.0 12.0 16.0 17.4 20.0 0.0

RJM	RKM	CNPSB	CNPSDB	CNPHDB	CNVB	LS	MPL	IZB	TETH	XIO(1)	RANGE
RJA	RKA	CLPSB	CLPSDB	CLPHDB	CLVB	WB	SB	IYB	MAS	XIO(2)	ALTITUDE
RJG	RKG	CYPSB	CYPSDB	CYPHDB	CYVB	WTC	DB	IYZB	THEO	XIO(3)	DYPRB
	RKB	DC	CDC								
24.7500	-42.8100	0.2260	-3.4900	-0.1700	-0.2260	5080.0	4.1	267400.0	1079.0	88.345	-50.7
9.7000	-46.5000	-0.0229	-0.4420	-0.3270	0.0229	3668.0	1700.0	54404.0	166.6	88.452	1120.4
23.2400	-41.2000	1.2900	2.1900	0.1420	-1.2900	97.7	41.2	2896.0	-1.415	88.658	0.041
	-45.6900	0.0434	1.1000								

ALPHA(I,J)

0.42E 06	-0.28E 06	-0.24E 07	-0.24E 07	-0.24E 07
-0.28E 06	0.57E 06	0.43E 07	0.43E 07	0.43E 07
-0.24E 07	0.43E 07	0.37E 08	0.37E 08	0.37E 08
-0.24E 07	0.43E 07	0.37E 08	0.37E 08	0.37E 08
-0.24E 07	0.43E 07	0.37E 08	0.37E 08	0.37E 08

BETA(I,J)

0.79E 05	0.31E 04	-0.72E 04	-0.72E 04	-0.72E 04
0.11E 05	0.54E 04	-0.10E 05	-0.10E 05	-0.10E 05
-0.50E 06	0.20E 06	0.20E 07	0.20E 07	0.20E 07
-0.50E 06	0.20E 06	0.20E 07	0.20E 07	0.20E 07
-0.50E 06	0.20E 06	0.20E 07	0.20E 07	0.20E 07

GAMMA(I,J)

0.12E 03	0.0	0.0	0.0	0.0
0.17E 03	0.81E 05	0.0	0.0	0.0
-0.33E 05	0.0	0.43E 06	0.0	0.0
-0.33E 05	0.0	0.0	0.44E 06	0.0
-0.33E 05	0.0	0.0	0.0	0.45E 06

COEFFICIENTS OF CHARACTERISTIC EQUATION IN ASCENDING ORDER

0.8490 24 0.5550 27 0.6790 28 0.1260 30 0.5100 30 0.2080 30 0.5270 30 0.5870 29 0.1150 30 0.2590 28 0.4430 28

ALL ROOTS HAVE BEEN ACCURATELY DETERMINED

ROOTS OF CHARACTERISTIC EQUATION REAL	IMAGINARY	STABILITY PARAMETERS NATURAL FREQUENCY	DAMPED FREQUENCY	DAMPING RATIO		TIME TO HALF OR DOUBLE AMPLITUDE
-0.2168D 0	0.2438D-19	0.2168D 00	0.2438D-19	0.1000D 01		0.3197D 01
-0.1904D-01	-0.6949D-01	0.7206D-01	0.6949D-01	0.2643D 00		0.3640D 02
-0.1904D-01	0.6949D-01	0.7206D-01	0.6949D-01	0.2643D 00		0.3640D 02
-0.8064D-01	-0.1130D 01	0.1133D 01	0.1130D 01	0.7116D-01		0.8596D 01
-0.8064D-01	0.1130D 01	0.1133D 01	0.1130D 01	0.7116D-01		0.8596D 01
-0.1558D-02	-0.2777D-23	0.1558D-02	0.2777D-23	0.1000D 01		0.4448D 03
-0.5356D-01	-0.2043D 01	0.2043D 01	0.2043D 01	0.2621D-01		0.1294D 02
-0.5356D-01	0.2043D 01	0.2043D 01	0.2043D 01	0.2621D-01		0.1294D 02
-0.2961D-01	-0.4513D 01	0.4514D 01	0.4513D 01	0.6561D-02	LIGHTLY DAMPED	0.2341D 02
-0.2961D-01	0.4513D 01	0.4514D 01	0.4513D 01	0.6561D-02	LIGHTLY DAMPED	0.2341D 02

Table VIII (Cont)

MODAL ANALYSIS

EIGENVECTOR REAL	IMAGINARY	MAGNITUDE	DIRECTION ANGLE	
0.1214E 00	-0.1663E-19	0.1214E 00	0.3600E 03	OVERDAMPED MODE
0.3928E-02	-0.3291E-21	0.3928E-02	0.3600E 03	
0.3849E-02	-0.3313E-21	0.3849E-02	0.3600E 03	
0.3797E-02	-0.3440E-21	0.3797E-02	0.3600E 03	
		2.1000E 01 ψ		
0.6597E-01	0.1135E 00	0.1312E 00 ϕ	0.5982E 02	FIRST MODE
0.1891E-01	0.1466E 00	0.1478E 00 σ_1	0.8265E 02	
0.1861E-01	0.1424E 00	0.1436E 00 σ_2	0.8255E 02	
0.1852E-01	0.1381E 00	0.1393E 00 σ_3	0.8236E 02	
0.6597E-01	-0.1135E 00	0.1312E 00	0.3002E 03	
0.1891E-01	-0.1466E 00	0.1478E 00	0.2774E 03	
0.1861E-01	-0.1424E 00	0.1436E 00	0.2774E 03	
0.1852E-01	-0.1381E 00	0.1393E 00	0.2776E 03	
0.1195E 02	0.1439E 03	0.1443E 03	0.8525E 02	
-0.1133E 01	-0.1011E 02	0.1018E 02	0.2636E 03	
-0.5647E 00	-0.6274E 01	0.6299E 01	0.2649E 03	
0.2599E 00	-0.4490E 00	0.5188E 00	0.3001E 03	
0.1195E 02	-0.1439E 03	0.1443E 03	0.2747E 03	
-0.1133E 01	0.1011E 02	0.1018E 02	0.9639E 02	
-0.5647E 00	0.6274E 01	0.6299E 01	0.9514E 02	
0.2599E 00	0.4490E 00	0.5188E 00	0.5994E 02	
-0.1967E-02	0.2162E-24	0.1967E-02	0.1800E 03	
0.7548E-01	-0.5482E-24	0.7548E-01	0.3600E 03	
0.7348E-01	-0.5408E-24	0.7348E-01	0.3600E 03	
0.7157E-01	-0.5404E-24	0.7157E-01	0.3600E 03	
-0.1144E 02	-0.1697E 00	0.1144E 02	0.1808E 03	
-0.3237E 02	-0.7342E 00	0.3237E 02	0.1813E 03	
0.1486E 01	0.3039E-01	0.1486E 01	0.1172E 01	
0.3240E 02	0.7303E 00	0.3241E 02	0.1291E 01	
-0.1144E 02	0.1697E 00	0.1144E 02	0.1792E 03	
-0.3237E 02	0.7342E 00	0.3237E 02	0.1787E 03	
0.1486E 01	-0.3039E-01	0.1486E 01	0.3588E 03	
0.3240E 02	-0.7303E 00	0.3241E 02	0.3587E 03	
-0.8399E 01	-0.1338E 00	0.8400E 01	0.1809E 03	
0.9251E 02	0.1443E 01	0.9253E 02	0.8933E 00	
-0.1868E 03	-0.2918E 01	0.1868E 03	0.1809E 03	
0.9546E 02	0.1495E 01	0.9547E 02	0.8972E 00	
-0.8399E 01	0.1338E 00	0.8400E 01	0.1791E 03	
0.9251E 02	-0.1443E 01	0.9253E 02	0.3591E 03	
-0.1868E 03	0.2918E 01	0.1868E 03	0.1791E 03	
0.9546E 02	-0.1495E 01	0.9547E 02	0.3591E 03	

TABLE IX

STABILITY ANALYSIS OF A TETHERED BALLOON IN THE LONGITUDINAL PLANE CASE 3 BJ BALLOON 70000. CU. FT.

ALTITUDE PROFILE	0.0	4713.0	5013.0	5313.0	5613.0	5913.0	7000.0	0.0
WIND VELOCITY PROFILE	6.0	6.0	8.0	12.0	16.0	17.4	20.0	0.0

ANGLE-OF-ATTACK(DEG)	-10.0000	-5.0000	0.0	5.0000	10.0000	15.0000	20.0000	25.0000
MOMENT COEFFICIENT	-0.2800	-0.1397	-0.0352	0.0595	0.5194	-0.0690	-0.2765	-0.7130
LIFT COEFFICIENT	-0.2100	-0.1150	-0.0200	0.0700	0.1600	0.2550	0.3450	0.4700
DRAG COEFFICIENT	0.0900	0.0650	0.0500	0.0500	0.0700	0.1100	0.1600	0.2500

THETA	XI0(1)	XI0(2)	XI0(3)
1.00000	86.99995	87.99995	88.99994
-1.36832	88.34862	88.46555	88.66144
-1.41481	88.34447	88.46161	88.65800
-1.41489	88.34447	88.46161	88.65800
-1.41494	88.34447	88.46161	88.65800
-1.41499	88.34447	88.46161	88.65800
-1.41495	88.34447	88.46161	88.65800
-1.41495	88.34441	88.46161	88.65800
FINAL SOLUTION			
-1.41496	88.34447	88.46161	88.65800

RJM	RKM	CMB	CMAB	CMTDB	LS	MPL	TETH	IXB
RJA	RKA	CLB	CLAB	CLTDB	WB	SB	DC	MAL
RJG	RKG	CDB	CDAB	CDTDB	WTC	DB	CDC	MAV
RJB	RKB	RANGE	ALTITUDE	DYPRB				
23.4200	-43.6200	-0.0648	1.1975	-3.2100	5080.	4.09	1079.	357404.
9.7000	-46.5000	-0.0469	1.0886	2.1100	3669.0	1700.0	0.0434	22.00
23.2400	-41.2000	0.0542	-0.1719	-0.0890	97.7	41.200	1.100	151.600
17.200	-45.690	-50.7	5833.4	0.290E 00				

ALPHA(I,J)

0.76E 06	-0.23E 07	-0.22E 07	-0.22E 07
-0.23E 07	0.18E 08	0.18E 08	0.18E 08
-0.22E 07	0.18E 08	0.18E 08	0.18E 08
-0.22E 07	0.18E 08	0.18E 08	0.18E 08

BETA(I,J)

0.18E 06	-0.55E 04	-0.55E 04	-0.55E 04
-0.11E 06	0.55E 06	0.52E 06	0.45E 06
-0.11E 06	0.52E 06	0.50E 06	0.45E 06
-0.11E 06	0.45E 06	0.45E 06	0.43E 06

GAMMA(I,J)

0.64E 05	0.0	0.0	0.0
-0.36E 05	0.42E 06	0.43E 02	0.66E 02
-0.36E 05	0.0	0.43E 06	0.69E 02
-0.35E 05	0.0	0.0	0.45E 06

COEFFICIENTS OF CHARACTERISTIC EQUATION IN ASCENDING ORDER

0.529D 22 0.332D 23 0.740D 24 0.206D 25 0.546D 25 0.110D 25 0.155D 25 0.603D 23 0.636D 23

ALL ROOTS HAVE BEEN ACCURATELY DETERMINED

ROOTS OF CHARACTERISTIC EQUATION REAL	IMAGINARY	STABILITY PARAMETERS NATURAL FREQUENCY	DAMPED FREQUENCY	DAMPING RATIO	TIME TO HALF OR DOUBLE AMPLITUDE
-0.1822D 00	0.3074D 00	0.3573D 00	0.3074D 00	0.5098D 00	0.3805D 01
-0.1822D 00	-0.3074D 00	0.3573D 00	0.3074D 00	0.5098D 00	0.3805D 01
-0.1363D-01	0.8960D-01	0.9063D-01	0.8960D-01	0.1504D 00	0.5085D 02
-0.1363D-01	-0.8960D-01	0.9063D-01	0.8960D-01	0.1504D 00	0.5085D 02
-0.1757D 00	0.1988D 01	0.1996D 01	0.1988D 01	0.8803D-01	0.3945D 01
-0.1757D 00	-0.1988D 01	0.1996D 01	0.1988D 01	0.8803D-01	0.3945D 01
-0.1033D 00	-0.4463D 01	0.4464D 01	0.4463D 01	0.2307D-01	0.6731D 01
-0.1033D 00	0.4463D 01	0.4464D 01	0.4463D 01	0.2307D-01	0.6731D 01

TABLE IX (Continued)

MODE SHAPES

EIGENVECTORS REAL	IMAGINARY	MAGNITUDE	DIRECTION ANGLE
0.4087E-01	-0.2848E-04	0.4087E-01	0.3600E 03
0.3871E-01	-0.3282E-03	0.3871E-01	0.3595E 03
0.3494E-01	0.2387E-03	0.3494E-01	0.3915E 00
0.4087E-01	0.2848E-04	0.4087E-01	0.3993E-01
0.3871E-01	0.3282E-03	0.3871E-01	0.4857E 00
0.3494E-01	-0.2387E-03	0.3494E-01	0.3596E 03
-0.1082E 01	0.3608E-01	0.1082E 01	0.1781E 03
-0.1049E 01	0.2489E-01	0.1050E 01	0.1786E 03
-0.1015E 01	-0.3572E-02	0.1015E 01	0.1802E 03
-0.1082E 01	-0.3608E-01	0.1082E 01	0.1819E 03
-0.1049E 01	-0.2489E-01	0.1050E 01	0.1814E 03
-0.1015E 01	0.3572E-02	0.1015E 01	0.1798E 03
-0.7087E 02	-0.3310E 02	0.7822E 02	0.2050E 03
0.9428E 00	0.2286E 01	0.2473E 01	0.6759E 02
0.7062E 02	0.3094E 02	0.7710E 02	0.2366E 02
-0.7087E 02	0.3310E 02	0.7822E 02	0.1550E 03
0.9428E 00	-0.2286E 01	0.2473E 01	0.2924E 03
0.7062E 02	-0.3094E 02	0.7710E 02	0.3363E 03
0.1765E 03	-0.2825E 02	0.1786E 03	0.3509E 03
-0.3537E 03	0.6224E 02	0.3592E 03	0.1700E 03
0.1778E 03	-0.3403E 02	0.1810E 03	0.3492E 03
0.1765E 03	0.2825E 02	0.1788E 03	0.9093E 01
-0.3537E 03	-0.6224E 02	0.3592E 03	0.1900E 03
0.1778E 03	0.3403E 02	0.1810E 03	0.1083E 02

Natural frequency	=	.072 rad/sec
Damped frequency	=	.069 rad/sec
Damping ratio	=	.264

The modal analysis (Table VIII) indicates that this is a coupled yaw lateral displacement mode (i.e., the tether link angles σ_1, σ_2 and σ_3 are approximately equal). Lateral displacement leads the balloon yaw motion by approximately 80 degrees. Table IX presents the longitudinal stability characteristics as added information. The experimental lateral response for Test Run No. 3 is again plotted in Figure 14 with additional data. The frequency of this motion is approximately 0.074 rad/sec as noted. The ratio of successive amplitudes of motion is

$$\frac{X_1}{X_2} = \frac{137}{62} = 2.21$$

The frequency of motion is in relatively good agreement with the small perturbation stability theory of .069 rad/sec damping ratio (ξ) which was predicted for the first lateral mode is .264 which corresponds to successive amplitude ratio as follows:

$$\delta = \frac{2\pi\xi}{\sqrt{1-\xi^2}} = \ln\frac{X_1}{X_2}$$

$$\delta = \frac{2 \times .264}{\sqrt{1-(.264)^2}} = 1.72$$

$$\frac{X_1}{X_2} = 5.59$$

The analytically predicted values of amplitude ratio are substantially higher than observed in the experimental data of Figure 14. However, a direct comparison can not be made inasmuch as forcing functions due to wind gusts effect the motion. In the stability theory, a free vibration condition is assumed.

A further attempt was made to deduce the probable wind fluctuations with time from the available flight test data. The relative wind which the balloon sees is a vectoral summation of the actual wind and the relative wind due to balloon

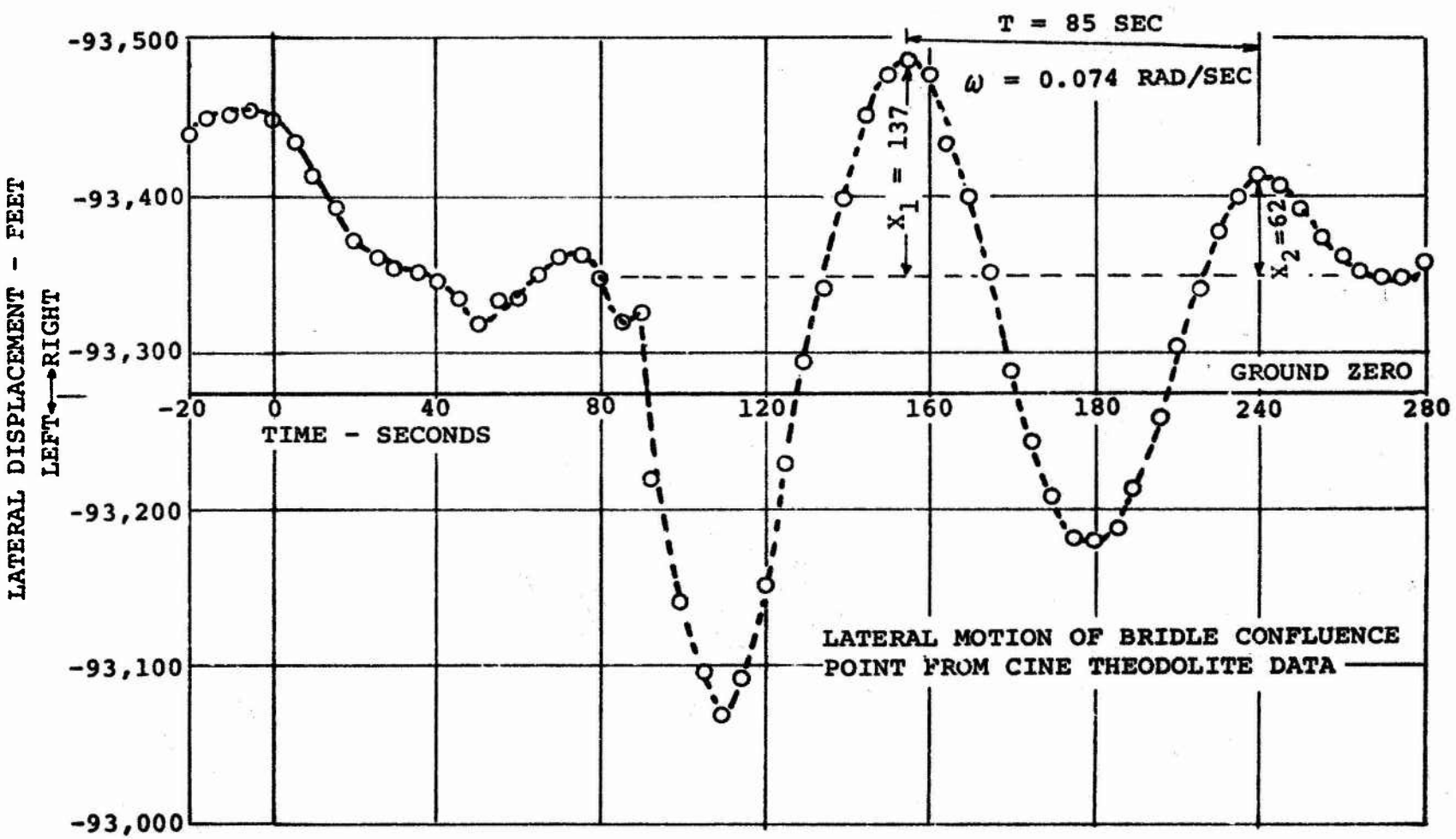

Figure 14. Time History of Lateral Displacement for Test Run No. 3

motion through the air mass. Balloon motion at the suspension line confluence point was observed by cinetheodolite. The magnitude of the relative wind at the confluence point was measured by means of a cup anemometer but direction of this relative wind is unknown. Assuming a constant value of the fore and aft wind relative to the tether point and the available data an attempt was made to calculate a possible lateral or side gust time history which might have existed during the test. A calculated balloon lateral response for this side gust time history did not correlate with the experimentally determined displacement.

In view of the inability to obtain a direct correlation between analytical predictions and experimental data, a more fundamental study was undertaken. This study consisted of an examination of the predicted response of the tethered balloon system to simple wind disturbances and an examination of the effects of aerodynamic damping on balloon motion.

The dynamic response of the balloon with a constant wind gust of 3 feet per second directed to the right after release of the balloon is plotted in Figures 15a, 15b and 15c. It is apparent in Figure 15a that the balloon's lateral displacement is retarded and more closely conforms to the actual motion observed during the first 60 seconds of the test. With the side gust maintained the balloon converges to a new yaw angle and the sideslip angle approaches zero (Figure 15b) as would be expected.

The nature of the experimental lateral displacement time history for Lateral Run No. 3 changes at 60 to 90 seconds as observed in Figure 14. It is considered that a change in wind direction or magnitude could excite the lateral motions of the tethered balloon system. A 3 fps side gust superimposed on a steady state 17 fps aft wind is approximately equivalent to a wind of constant magnitude but shifted in azimuth by 10 degrees. This wind change could be consistent with the light and variable winds existing during the time of the test. Consequently, it was chosen to further investigate the dynamic behavior of the test balloon system.

The experimental yaw angle of the balloon during the test (Figure 16) can be used to obtain initial conditions for digital computer simulation of the mathematical model. From Figure 16 at time 63 seconds yaw angle (ψ) is zero and the yawing velocity ($\dot{\psi}$) is -2.7 degrees per second. (i.e., nose rotating to left when looking down on the balloon). From cinetheodolite data the suspension line confluence point is moving to the right at +3.0 fps. A dynamic simulation of the balloon motion was obtained with these initial conditions and a forcing function consisting of a side gust of 3 fps to the

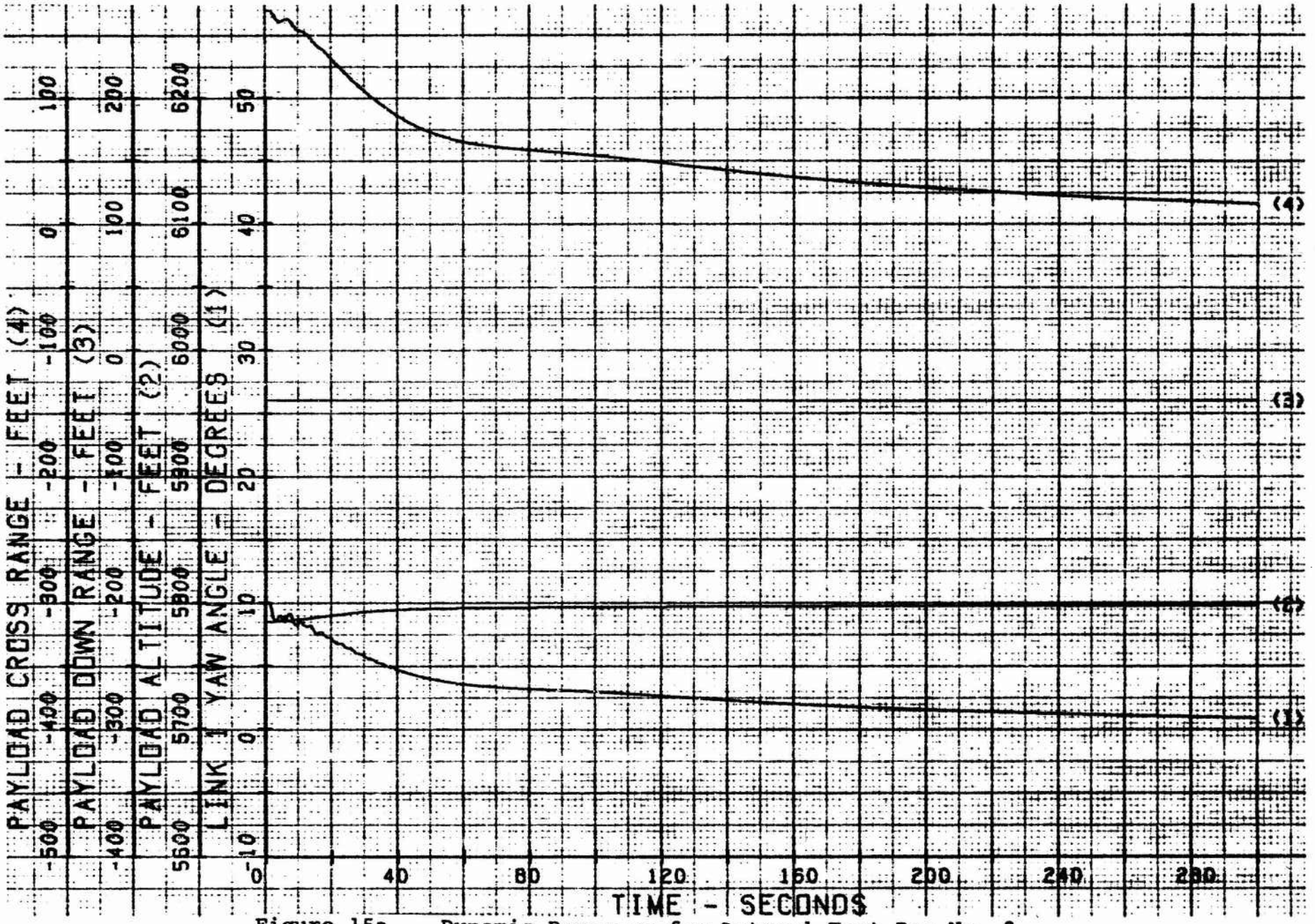

Figure 15a. Dynamic Response for Lateral Test Run No. 3
Constant Lateral Wind Gust of 3 fps to Right

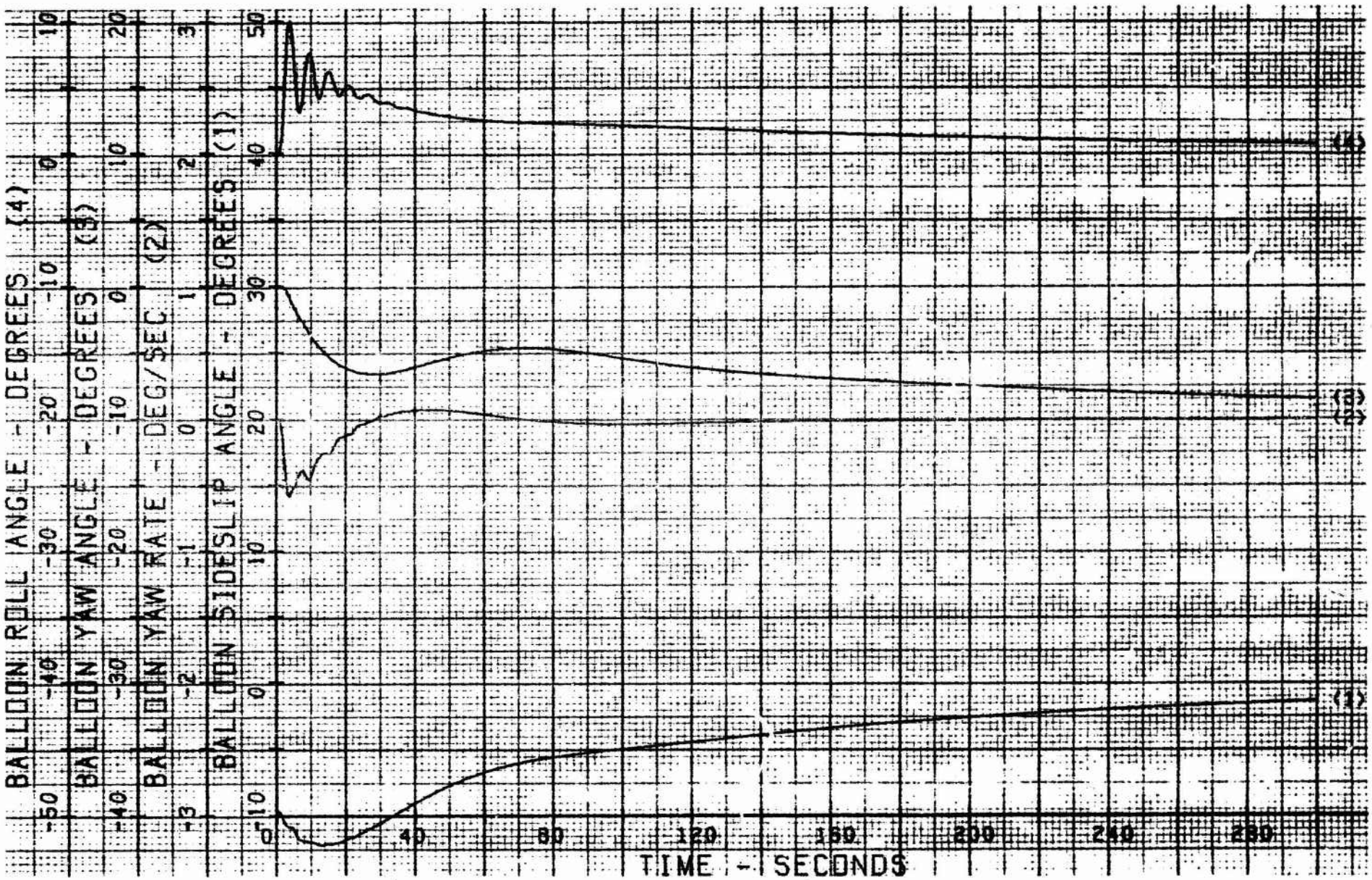

Figure 15b. Dynamic Response for Lateral Test Run No. 3
Constant Lateral Wind Gust of 3 fps to Right

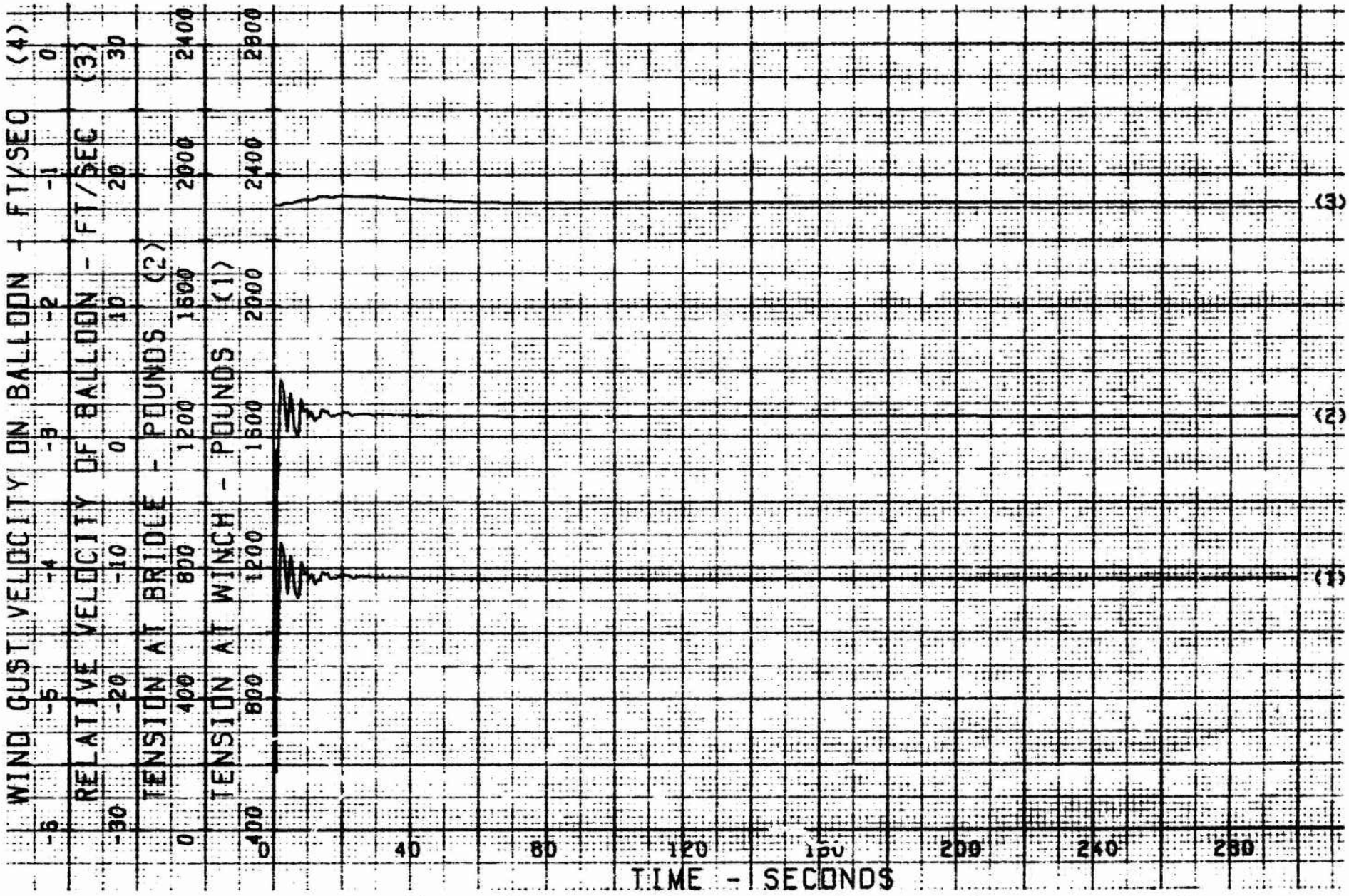

Figure 15c. Dynamic Response for Lateral Test Run No. 3
Constant Lateral Wind Gust of 3 fps to Right

FIGURE 16

MEASURED YAW
TETHERED BALLOON SYSTEM
TEST 3 LATERAL BALLOON DISPLACEMENT OF 150 FT TO RIGHT
TETHER LENGTH 1086 FT.

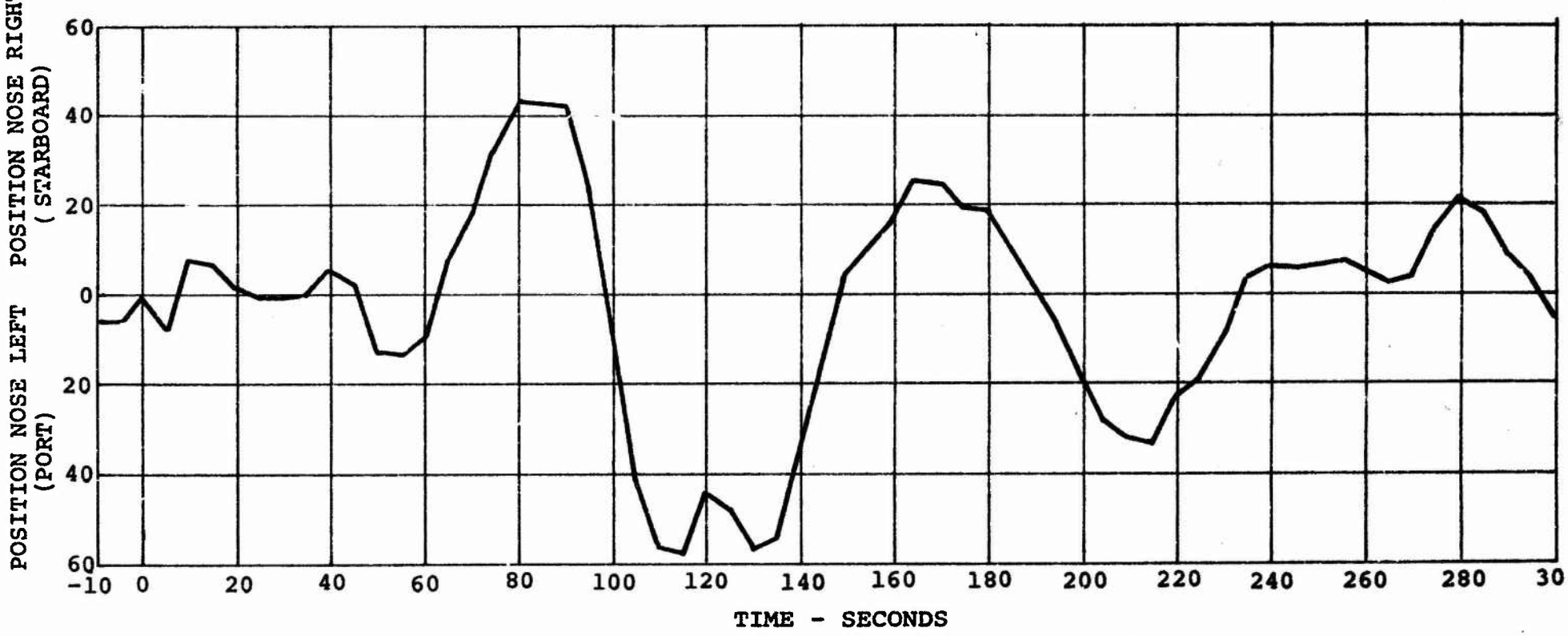

left with a duration of 40 seconds.

The lateral response of the tethered balloon system to this disturbance is duplicated in Figures 17a, 17b and 17c. A comparison of simulated and experimental lateral balloon motion shows some similarities and some differences. Consider one cycle of motion from 110 seconds on after the forcing function has been removed. The simulated motion has a period of 98 seconds or a frequency of 0.064 rad/sec and the experimental motion has a period of 90 seconds or a frequency of 0.070 rad/sec. These results are in close agreement. The stability and modal analysis for this balloon system (Table IX) also identifies this motion as the first mode with a frequency of .069 rad/sec. The mode is a coupled yaw-lateral displacement with the lateral displacement lagging the yawing motion.

It is also apparent in comparing experimental data and the dynamic simulation that the simulated motion at this frequency is more highly damped. An additional mode of motion is apparent in the simulation after the first mode has damped out. This mode is a slow convergence of balloon yaw and lateral displacement to the initial equilibrium position. Again, examination of the model, analysis of Table IX reveals an overcritically damped mode with balloon yaw motion and lateral displacement in phase.

The highly damped first mode indicated by the dynamic simulation is not in accordance with the observed response. This might be attributed to the accuracy with which aerodynamic damping characteristics can be determined by calculations or the inability to input the proper forcing functions. Considering the former further calculations were made with the dynamics computer simulation program to determine the effects of aerodynamic damping on system motion. The effect of reducing aerodynamic damping coefficients on lateral motion is shown in Figure 18. The lateral displacement has been obtained with a 3 fps side gust as before and the six lateral aerodynamic damping coefficients have been reduced to percentages of 100% damping presented in Section III. Although static lateral aerodynamic data were not available for angles of sideslip greater than 20 degrees a projection of possible aerodynamic characteristics (Figure 19) was made to permit dynamic simulation at larger angles. It is apparent that lateral balloon motion is quite sensitive to aerodynamic damping.

In Figure 18 a reduction in aerodynamic damping was shown to have a very significant effect on the lateral dynamics of the tethered balloon. In fact, at a point between 81% and 85% of the estimated damping the lateral motion becomes unstable. Lateral stability computer runs were made with damping coefficients reduced by as much as 20%; and although the roots of the

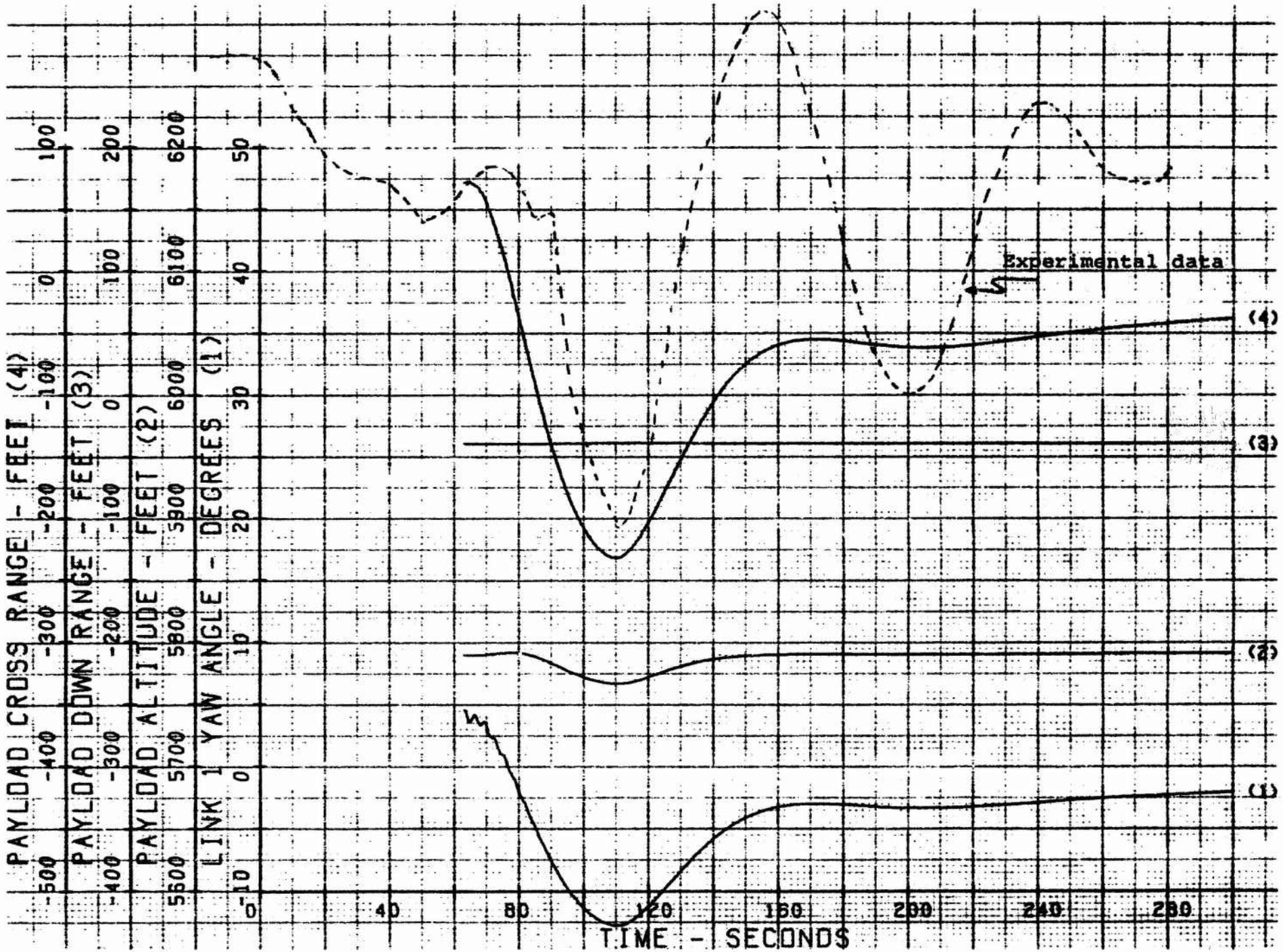

Figure 17a. Lateral Dynamic Response of Test Balloon to a 3 fps Side Gust of 40 Seconds Duration

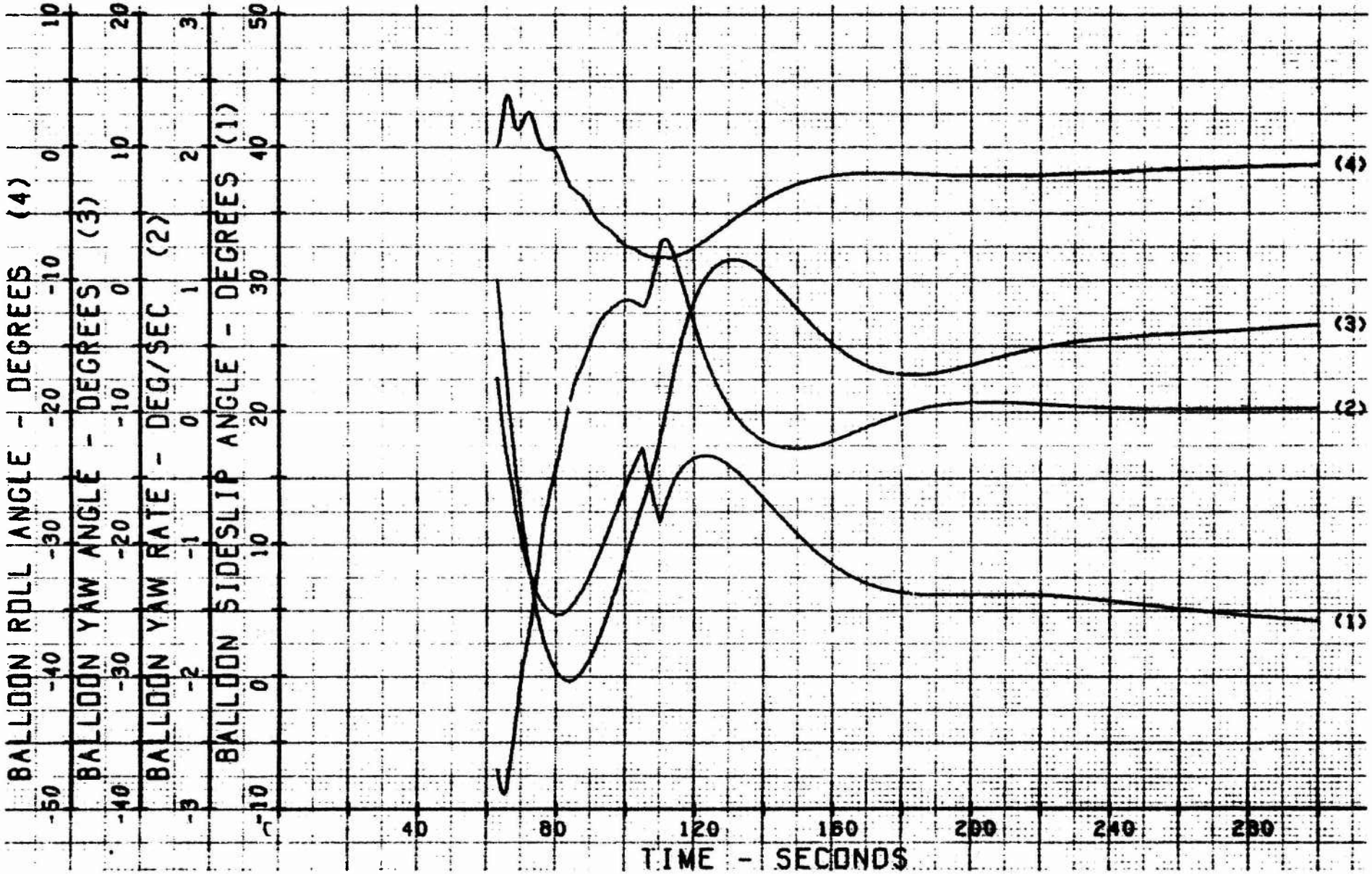

Figure 17b. Lateral Dynamic Response of Test Balloon to a 3 fps Side Gust of 40 Seconds Duration

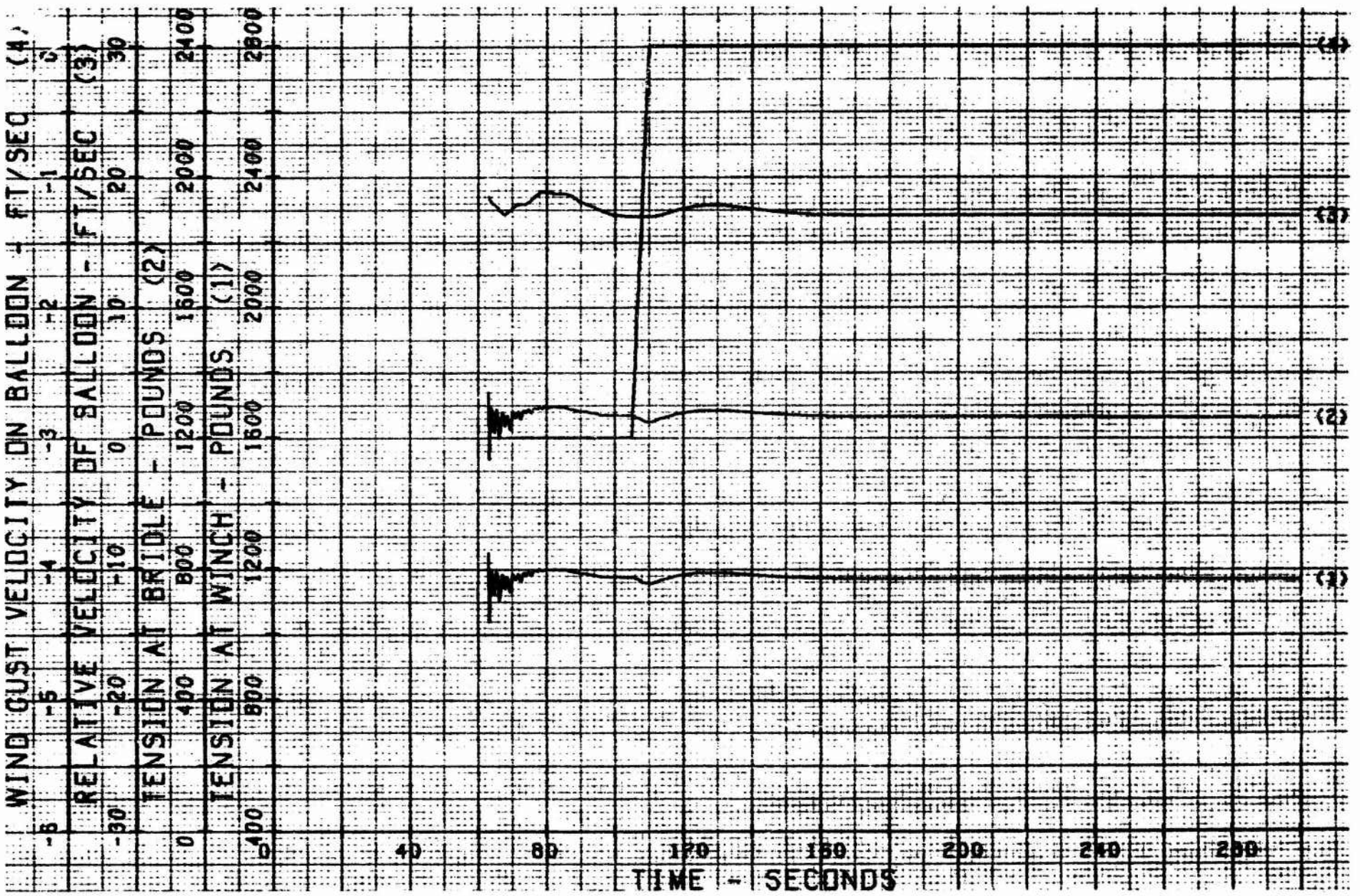

Figure 17c. Lateral Dynamic Response of Test Balloon to a 3 fps Side Gust of 40 Seconds Duration

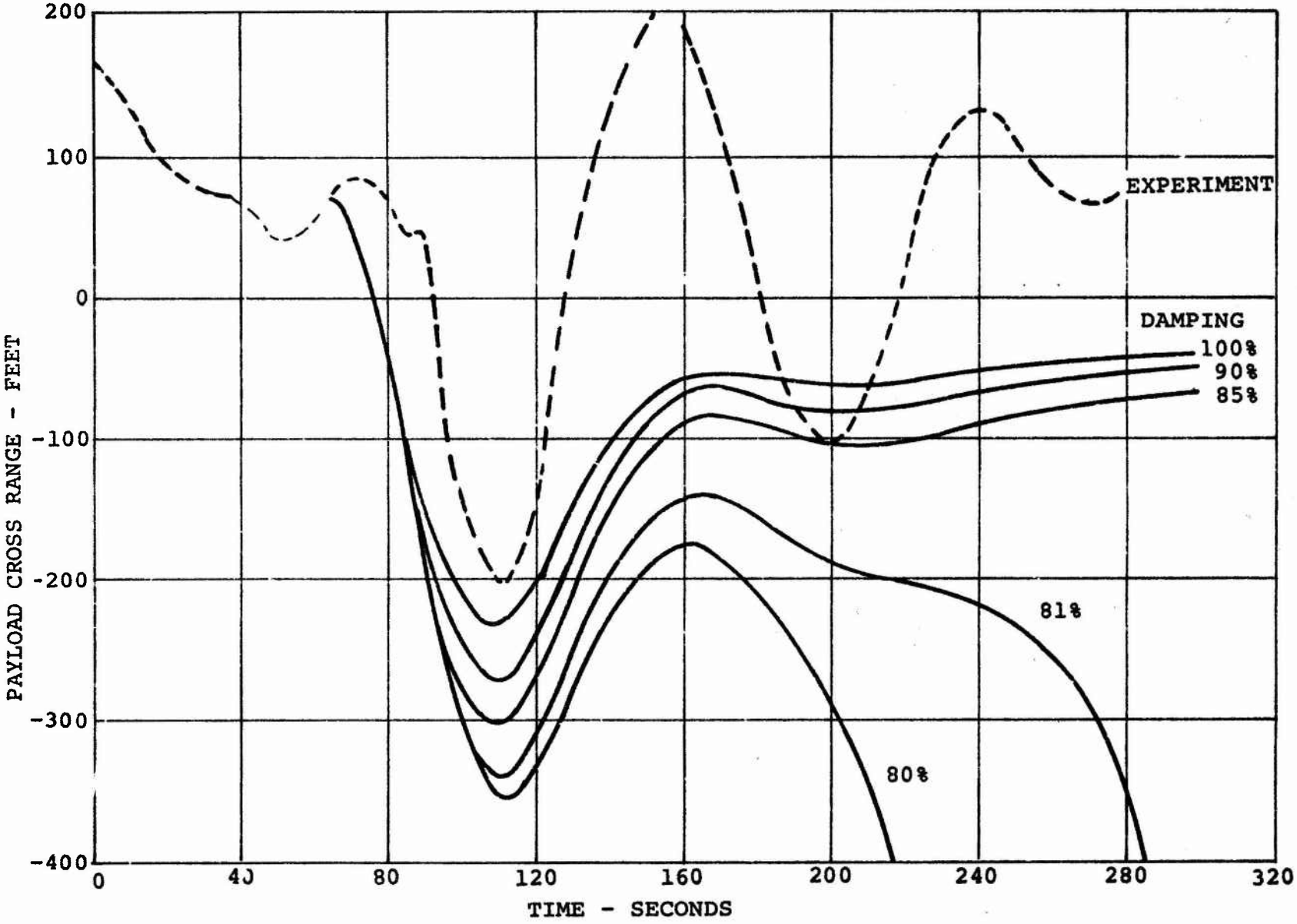

Figure 18. Lateral Displacement of Balloon as a Function of Aerodynamic Damping

ASSUMPTIONS

1. LIFT (C_L) DATA AVAILABLE AT LARGE ANGLES OF ATTACK ARE INDICATIVE OF NATURE OF SIDE FORCE (C_y).

2. YAW MOMENT (C_n) AND ROLL MOMENT (C_ℓ) IS DIRECTLY PROPORTIONAL TO SIDE FORCE (C_y).

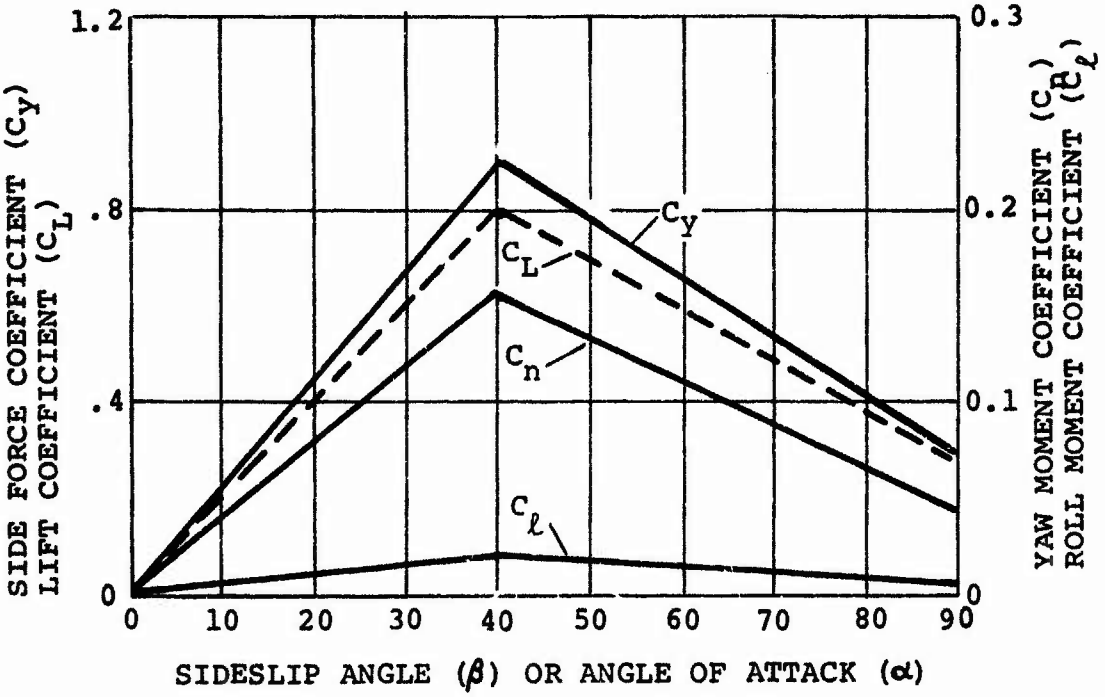

Figure 19. Estimate of Static Lateral Aerodynamic Coefficients at Large Sideslip Angles

characteristic equation become less stable, they give no indication of the unstable motion encountered in the dynamic simulation. This points out an inadequacy of the stability program. Although a balloon can be designed to be stable near its equilibrium position, it may develop motions far away from equilibrium which are unstable. It should be pointed out that the damping coefficients are considered to be invariant from this equilibrium condition. In reality they would vary, possibly enough to prevent the unstable motion shown in the simulation.

SECTION VI

CONCLUSIONS AND RECOMMENDATIONS

Digital computer programs were developed previously to describe tethered balloon stability qualities and to simulate dynamic motions of tethered balloon systems. Experimental test conditions and test tethered balloon characteristics were input in the computer programs and balloon dynamic behavior was predicted. A comparison of experimental and predicted results permits establishing the validity of these mathematical tools. The following conclusions are drawn from this program.

1. Experimental and predicted longitudinal dynamic behavior are in reasonable agreement. The experiment clearly excites the first mode of motion with a frequency as predicted by stability theory. This mode is a coupled motion of balloon pitch and fore and aft motion of the tether as a whole (180 degrees out of phase). Damping of the fore and aft motion is greater in the real world and may be attributed in part to the fact that yawing motions existed and would contribute to greater aerodynamic drag forces.

2. The experiments, even though carefully controlled to excite longitudinal and lateral motions independently, result in coupled tethered balloon system motions. This may be attributed in part to the light and variable winds. It is apparent that the lateral motion of the test balloon in particular is sensitive to wind changes.

3. It is more difficult to establish correlation of experimental and predicted lateral motions than longitudinal motions.

4. The stability analysis and dynamic simulation identify two lateral modes of motion which are excited. The first lateral mode is a coupled yaw-lateral displacement with the lateral displacement lagging the yawing motion. The frequency of this mode is in good agreement with experimental measurements. The second mode is a highly damped mode with balloon yaw motion and lateral displacement in phase.

5. Discrepancies between experimental and predicted lateral motions may be attributed to undefined wind forcing functions and the accuracy with which aerodynamic damping coefficients can be calculated. Analysis indicates that lateral motions can be relatively sensitive to aerodynamic damping.

6. The comparison of experimental and predicted dynamic characteristics of the tethered balloon shows a reasonable match although some discrepancies do exist. In spite of these,

stability and dynamic simulation computer programs are a powerful tool for design and analysis of tethered balloon systems.

As a result of this program the following recommendations are made:

1. For future analysis, obtain additional and more accurate data for tethered balloon systems of interest. Additional aerodynamic data, particularly aerodynamic damping data, may be obtained with dynamic wind tunnel models. Additional field testing with accurately determined time histories of wind magnitude and direction might also permit deduction of aerodynamic damping characteristics.

2. It is recognized that some limitations exist in the present dynamic simulation techniques as a result of treating the longitudinal and lateral motions as uncoupled. It is recommended that the mathematical model be extended to be completely three dimensional and that provisions for a wind vector changing in direction and magnitude as a function of time be incorporated.

REFERENCES

1. AFCRL-71-0213, Scientific Report No. 1, "Definition of Tethered Balloon Systems," Myers, P.F. and Vorachek, J.J., 31 March 1971. A.D. No. 725,708

2. AFCRL-71-0406, "Investigation of Stability Characteristics of Tethered Balloon Systems," Doyle, G.R. and Vorachek, J.J., 30 July 1971. A.D. No. 731,570

3. AFCRL-72-0113, "Investigation of Dynamic Behavior of Tethered Balloon Systems," Vorachek, J.J., Burbick, J.W. and Doyle, G.R., 31 January 1972. A.D. No. 740,723

4. 70,000 Cubic Foot Balloon Operation and Maintenance Handbook.

5. Report No. Mech. Eng. 24. "Ballonet Kite Balloons Design, Construction and Operation," Brown, I.S.H. and Speed, L.A., Royal Aircraft Establishment, July, 1962.

6. Lamb, Sir Horace: Hydrodynamics, 6th Edition, The University Press, Cambridge, England, 1932.

7. Munk, Max: Fundamentals of Fluid Dynamics for Aircraft Designers, Ronald Press Company, New York, 1929.

8. Perkins, Courtland D. and Hage, Robert E: Airplane Performance, Stability, and Control, Wiley, New York, 1949.

9. Aerodynamic Coefficients of Four Balloon Shapes at High Attack Angles; Peters, Penn A.; Shindo, Shojiro; Lysons, Hilton H. Presented at AFCRL Scientific Balloon Symposium, September 1972.

10. University of Washington Aeronautical Laboratory Report 957F, "Analysis and Discussion of Aerodynamic Characteristics of Balloons Tested in a Wind Tunnel," Shindo, Shojiro, August 24, 1970.

11. University of Washington Aeronautical Laboratory Report 957G, "A Wind Tunnel Test of a Single Hulled Balloon - Lateral Aerodynamic Characteristics," Shindo, Shojiro, March 29, 1971.